Title: Outer membrane lipid homeostasis via retrograde phospholipid transport in *Escherichia coli*

Authors: Rahul Shrivastava[a], Xiang'Er Jiang[b], Shu-Sin Chng[a,b*]

Affiliations:

[a]Department of Chemistry, National University of Singapore, Singapore 117543.

[b]Singapore Center for Environmental Life Sciences Engineering, National University of Singapore (SCELSE-NUS), Singapore 117456.

*To whom correspondence should be addressed. E-mail: chmchngs@nus.edu.sg

The authors declare no conflict of interest.

Abstract

The outer membrane (OM) is essential for viability in Gram-negative bacteria, yet mechanisms to ensure its stability and homeostasis are not understood. The trans-envelope Tol-Pal complex, whose physiological role has remained elusive, is important for OM stability. Here, we establish that the Tol-Pal complex is required for PL transport and OM lipid homeostasis in *Escherichia coli*. Cells lacking the complex exhibit defects in lipid asymmetry and accumulate excess phospholipids (PLs) in the OM. This imbalance in OM lipids is due to defective retrograde PL transport in the absence of a functional Tol-Pal complex. Thus, cells ensure the assembly of a stable OM by maintaining an excess flux of PLs to the OM only to return the surplus to the inner membrane. Our findings also provide insights into the mechanism by which the Tol-Pal complex may promote OM invagination during cell division.

Keywords

outer membrane stability; membrane homeostasis; lipid trafficking; membrane lipid asymmetry; membrane contact sites; TolQRA

Introduction

Lipid bilayers define cellular compartments, and thus life itself, yet our understanding of the assembly and maintenance of these structures are limited. In Gram-negative bacteria, the outer membrane (OM) is essential for growth, and allows the formation of an oxidizing periplasmic compartment beyond the cytoplasmic or inner membrane (IM) (Nikaido, 2003). The OM is asymmetric, with lipopolysaccharides (LPS) and phospholipids (PLs) found in the outer and inner leaflets, respectively. This unique lipid asymmetry is required for the OM to function as an effective and selective permeability barrier against toxic substances, rendering Gram-negative bacteria intrinsically resistant to many antibiotics, and allowing survival under adverse conditions. The assembly pathways of various OM components, including LPS (Okuda et al., 2016), β-barrel OM proteins (OMPs) (Hagan et al., 2011), and lipoproteins (Okuda and Tokuda, 2011), have been well-characterized; however, processes by which PLs are assembled into the OM have not been discovered. Even though they are the most basic building blocks of any lipid bilayer, essentially nothing is known about how PLs are transported between the IM and the OM. Unlike other OM components, PL movement between the two membranes is bidirectional (Donohue-Rolfe and Schaechter, 1980; Jones and Osborn, 1977; Langley et al., 1982). While anterograde (IM-to-OM) transport is essential for OM biogenesis, the role for retrograde (OM-to-IM) PL transport is unclear. How assembly of the various OM components are coordinated to ensure homeostasis and stability of the OM is also unknown.

The Tol-Pal complex is a trans-envelope system highly conserved in Gram-negative bacteria (Lloubes et al., 2001; Sturgis, 2001). It comprises five proteins organized in two sub-complexes, TolQRA in the IM and TolB-Pal at the OM. In *Escherichia coli*, these sub-complexes interact in a proton motive force (pmf)-dependent fashion, with TolQR transducing

energy to control conformational changes in TolA and allowing it to reach across the periplasm to contact Pal (Cascales et al., 2000; Germon et al., 2001), an OM lipoprotein that binds peptidoglycan (Godlewska et al., 2009). TolA also interacts with periplasmic TolB (Walburger et al., 2002), whose function within the complex is not clear. The TolQRA sub-complex is analogous to the ExbBD-TonB system (Lloubes et al., 2001; Cascales et al., 2001; Witty et al., 2002), where energy-dependent conformational changes in TonB are exploited for the transport of metal-siderophores across the OM (Gresock et al., 2015). Unlike the ExbBD-TonB system, however, the physiological role of the Tol-Pal complex has not been elucidated, despite being discovered over four decades ago (Bernstein et al., 1972; Lazzaroni and Portalier, 1981). The Tol-Pal complex has been shown to be important for OM invagination during cell division (Gerding et al., 2007), but mutations in the *tol-pal* genes also result in a variety of phenotypes, such as hypersensitivity to detergents and antibiotics, leakage of periplasmic proteins, and prolific shedding of OM vesicles, all indicative of an unstable OM (Lloubes et al., 2001). In addition, removing the *tol-pal* genes causes envelope stress and up-regulation of the σ^E and Rcs phosphorelay responses (Vines et al., 2005; Clavel et al., 1996). It has thus been suggested that the Tol-Pal complex may in fact be important for OM stability and biogenesis. Interestingly, the *tol-pal* genes are often found in the same operon as *ybgC* (Sturgis, 2001), which encodes an acyl thioesterase shown to interact with PL biosynthetic enzymes in *E. coli* (Gully and Bouveret, 2006). This association suggests that the Tol-Pal complex may play a role in PL metabolism and/or transport.

Here, we report that the Tol-Pal complex is required for retrograde PL transport and OM lipid homeostasis in *E. coli*. We show that cells lacking the Tol-Pal complex exhibit defects in OM lipid asymmetry, as judged by the presence of outer leaflet PLs. We further demonstrate that *tol-pal* mutants accumulate excess PLs (relative to LPS) in the OM, indicating lipid imbalance in

the membrane. Finally, using OM PL turnover as readout, we establish that the Tol-Pal complex is functionally important for efficient transport of PLs from the OM back to the IM. Our work solves a longstanding question on the physiological role of the Tol-Pal complex, and provides novel mechanistic insights into lipid homeostasis in the OM.

Results

Cells lacking the Tol-Pal complex exhibit defects in OM lipid asymmetry

To elucidate the function of the Tol-Pal complex, we set out to characterize the molecular nature of OM defects observed in *tol-pal* mutants in *E. coli*. Defects in the assembly of OM components typically lead to perturbations in OM lipid asymmetry (Wu et al., 2006; Ruiz et al., 2008). This is characterized by the accumulation of PLs in the outer leaflet of the OM, which serve as substrates for PagP-mediated acylation of LPS (lipid A) (Bishop, 2005). To determine if *tol-pal* mutants exhibit defects in OM lipid asymmetry, we analyzed lipid A acylation in strains lacking any member of the Tol-Pal complex. We demonstrated that each of the mutants accumulate more hepta-acylated lipid A in the OM compared to wild-type (WT) cells (Figure 1). This OM defect, and the resulting SDS/EDTA sensitivity in these *tol-pal* mutants, are all corrected in the complemented strains (Figure 1 - figure supplement 1). We also examined other strains with known OM permeability defects. We detected increased lipid A acylation in strains with either impaired OMP (*bamB*, *bamD*, Δ*surA*) or LPS (*lptD4213*) biogenesis, as would be expected, but not in strains lacking covalent tethering between the cell wall and the OM (Δ*lpp*) (Figure 1). Even though the Δ*lpp* mutant is known to exhibit pleiotropic phenotypes (Yem and Wu, 1978; Bernadac et al., 1998), it does not have perturbations in OM lipid asymmetry. In contrast to OMP or LPS assembly mutants, *tol-pal* strains produce WT levels of major OMPs

and LPS in the OM (Figure 1 - figure supplement 2). These results indicate that *tol-pal* mutations lead to accumulation of PLs in the outer leaflet of the OM independent of OMP and LPS biogenesis pathways.

Cells lacking the Tol-Pal complex have disrupted OM lipid homeostasis

We hypothesized that the loss of OM lipid asymmetry in *tol-pal* mutants is due to defects in PL transport across the cell envelope. To test this, we examined the steady-state distribution of PLs (specifically labelled with [^{3}H]-glycerol) between the IM and the OM in WT and *tol-pal* strains. We established that *tol-pal* mutants have ~1.4-1.6-fold more PLs in their OMs (relative to the IMs) than the WT strain (Figure 2A and Figure 2 - figure supplement 2). To ascertain if this altered distribution of PLs between the two membranes was due to the accumulation of more PLs in the OMs of *tol-pal* mutants, we quantified the ratios of PLs to LPS (both lipids now labelled with [^{14}C]-acetate) following OM isolation and differential extraction. *tol-pal* mutants contain ~1.5-2.5-fold more PLs (relative to LPS) in their OMs, when compared to the WT strain (Figure 2B and Figure 2 - figure supplement 3). Since *tol-pal* mutants produce WT LPS levels (Figure 1 - figure supplement 2B), we conclude that strains lacking the Tol-Pal complex accumulate excess PLs in their OMs, a phenotype that can be corrected via genetic complementation (Figure 2). Consistent with this idea, *tol-pal* mutants, unlike WT (Fuhrer et al., 2006), are able to survive the toxic effects of LPS overproduction (Figure 2 - figure supplement 4), possibly due to a more optimal balance of PLs to LPS in their OMs. Importantly, having excess PLs makes the OM unstable, which can account for increased permeability of the OM in *tol-pal* mutants (Lloubes et al., 2001). It also explains why these strains produce more OM vesicles (~34-fold higher than WT cells, albeit only at ~5% of total membranes (Figure 2 - figure supplement 5))(Bernadac et al., 1998). Furthermore, cells lacking the Tol-Pal complex are on

average shorter and wider than WT cells (when grown under conditions with no apparent division defects) (Gerding et al., 2007); this reflects an increase in surface area of the rod-shaped cells, perhaps a result of increase in OM lipid content. As expected, we did not observe disruption of lipid homeostasis in the Δ*lpp* mutant (Figure 2). However, we observed higher PL content in the OMs of strains defective in OMP assembly. We reasoned that this increase may help to stabilize the OM by filling the voids created by the decrease in properly-assembled OMPs. Since strains lacking the Tol-Pal complex have proper OMP assembly (Figure 1 - figure supplement 2A), the phenotype of excess PL build-up in the OM must be due to a different problem. Our results suggest that *tol-pal* mutations directly affect PL transport processes, and therefore OM lipid homeostasis.

Cells lacking the Tol-Pal complex are defective in retrograde PL transport

Unlike for other OM components, PL transport between the IM and the OM is bidirectional (Donohue-Rolfe and Schaechter, 1980; Jones and Osborn, 1977; Langley et al., 1982). Therefore, a simple explanation for the accumulation of excess PLs in the OMs of cells lacking the Tol-Pal complex is that there are defects in retrograde PL transport. To evaluate this possibility, we used the turnover of OM PLs (specifically anionic lipids, including phosphatidylserine (PS), phosphatidylglycerol (PG), and cardiolipin (CL)) as readout for the transport of PLs back to the IM (Figure 3A). As an intermediate during the biosynthesis of the major lipid phosphatidylethanolamine (PE), PS is converted to PE by the PS decarboxylase (PSD) at the IM, and typically exists only at trace levels (Cronan, 2003). PG and CL have relatively short lifetimes (Kanfer and Kennedy, 1963; Kanemasa et al., 1967). While the pathways for CL turnover are not known, PG can be converted to PE via PS (Yokoto and Kito, 1982). Since all known enzymes involved in possible pathways of converting PG to PS, and then

151 to PE, are localized in the IM (Cronan, 2003), the turnover of OM anionic lipids require, and
152 therefore report on, retrograde PL transport. Such an assay has previously been employed to
153 demonstrate retrograde transport for PS (Langley et al., 1982).

154 Using a strain expressing a temperature-sensitive (Ts) allele (*psd2*) of the gene encoding
155 PSD (Hawrot and Kennedy, 1978), we pulse-labelled PLs with [^{32}P]-phosphate at the restrictive
156 temperature (42˚C), and monitored the turnover of individual PL species in the OM during a
157 chase period at the permissive temperature (30˚C). At 42˚C, the *psd2* strain accumulates
158 substantial amounts of PS in both the IM and the OM (Figure 3B, 0-min time point), as
159 previously reported (Hawrot and Kennedy, 1978). With the restoration of PSD activity at 30˚C,
160 we observed initial increase but eventual conversion of PS to PE in both membranes (Figure 3B,
161 after 45-min time point), indicating that OM PS is transported back to the IM, converted to PE,
162 and subsequently re-equilibrated to the OM (Langley et al., 1982). We also detected higher
163 PG/CL content in the *psd2* strain at 42˚C, and saw rapid conversion of these lipids to PE in both
164 membranes at 30˚C (Figure 3B), at rates comparable to what was previously reported (for PG)
165 (Yokoto and Kito, 1982). The fact that PS levels increase initially but decrease after 45 min into
166 the chase is consistent with the idea that PS is an intermediate along the turnover pathway for PG
167 (Yokoto and Kito, 1982), as well as for CL. To confirm this observation, we also performed the
168 chase at 42˚C in the presence of a known PSD inhibitor (Satre and Kennedy, 1978) (these
169 conditions completely shut down PSD activity), and found quantitative conversion of PG/CL to
170 PS in both membranes (Figure 3 - figure supplement 1). We further showed that PG/CL-to-PE
171 conversion is abolished in the presence of the pmf uncoupler carbonyl cyanide *m*-chlorophenyl
172 hydrazone (CCCP) (Figure 3C), demonstrating that cellular energy sources are required for this
173 process (Yokoto and Kito, 1982), and that conversion occurs in the IM. The observation of
174 PG/CL turnover in the IM is thus expected. The fact that we also observed the conversion of OM

175 PG/CL to PE points towards an intact retrograde PL transport pathway for these lipids in the
176 otherwise WT cells. Notably, turnover of OM PG/CL appears to be slightly faster than that of IM
177 PG/CL (Figure 3B), suggesting that retrograde transport of these lipids may be coupled to the
178 turnover process.

179 We performed the same pulse-chase experiments with *psd2* cells lacking TolA. We
180 detected PG/CL-to-PE conversion in the IM at rates comparable to WT (Figure 3D and F; ~67%
181 and ~71% PG/CL turnover at 2 h-chase in Δ*tolA* and WT IMs, respectively (Figure 4A)),
182 demonstrating that there are functional PG/CL turnover pathways in the Δ*tolA* mutant. In
183 contrast, we observed substantial reduction of the turnover of OM PG/CL in these cells (Figure
184 3D and F; ~53% PG/CL turnover at 2 h-chase in the Δ*tolA* OM, compared to ~79% for WT
185 (Figure 4A)), even though PS conversion to PE appears intact. These results indicate an apparent
186 defect in the movement of PG and CL (but not PS) from the OM back to the IM, which is
187 restored when complemented with functional $tolA_{WT}$ (Figure 3E and F and Figure 4A). Δ*tolR*
188 mutant cells exhibit the same defect, and can similarly be rescued by complementation with
189 functional $tolR_{WT}$ (Figure 4A). In contrast, no rescue was observed when Δ*tolR* was
190 complemented using a *tolR* allele with impaired ability to utilize the pmf ($tolR_{D23R}$) (Cascales et
191 al., 2001) (Figure 4A and Figure 1 - figure supplement 1); this indicates that Tol-Pal function is
192 required for efficient PG/CL transport. We also examined PG/CL turnover in *psd2* cells lacking
193 BamB, which accumulate excess PLs in the OM due to defects in OMP assembly (Figure 2).
194 Neither IM nor OM PG/CL turnover is affected (Figure 4A), highlighting the different basis for
195 OM PL accumulation in this strain compared to the *tol-pal* mutants. Our assay does not report on
196 the retrograde transport of major lipid PE, which is relatively stable (Kanfer and Kennedy,
197 1963). However, since *tol-pal* mutants accumulate ~1.5-fold more PLs in the OM (Figure 2)
198 without gross changes in PL composition (compared to WT) (Figure 2 - figure supplement 6), PE

transport must also have been affected. We conclude that the Tol-Pal complex is required for the retrograde transport of bulk PLs in *E. coli*.

Overexpressing a putative PL transport system partially rescues defects in retrograde PL transport observed in *tol-pal* mutants

Removing the Tol-Pal complex does not completely abolish retrograde PG/CL transport, indicating that there are other systems involved in this process. The OmpC-Mla system is important for the maintenance of OM lipid asymmetry, and is proposed to do so via retrograde PL transport (Malinverni and Silhavy, 2009; Chong et al., 2015). To determine if this system plays a major role in retrograde PL transport in cells lacking the Tol-Pal complex, we examined OM PG/CL turnover in Δ*tolA* cells also lacking MlaC, the putative periplasmic lipid chaperone of the system. We first showed that cells lacking MlaC alone do not exhibit defects in OM PG/CL turnover (Figure 4A). Evidently, removing MlaC also does not exacerbate the defects in retrograde PL transport in cells lacking the Tol-Pal complex, given that overall turnover rates of IM and OM PG/CL are similarly reduced in the double mutant. These results indicate that the OmpC-Mla system does not contribute significantly to retrograde transport of bulk lipids when expressed at physiological levels, as has been previously suggested (Malinverni and Silhavy, 2009). We also tested whether overexpressing the OmpC-Mla system can restore retrograde PL transport in *tol-pal* mutants. Interestingly, overexpression of MlaC and the IM MlaFEDB complex (Thong et al., 2016), but not MlaA, partially rescues OM PG/CL turnover in the Δ*tolA* mutant (Figure 4B). However, this has no consequential effect on alleviating permeability defects observed in the Δ*tolA* strain (Figure 4B and Figure 4 - figure supplement 2), presumably because the OmpC-Mla system may have higher specificity for PG (Thong et al., 2016). Since PE is the predominant PL species in the OM (Figure 2 - figure supplement 6) (Cronan, 2003),

overexpressing the OmpC-Mla system may not effectively reduce the overall build-up of PLs caused by the loss of Tol-Pal function. Further to validating the putative PL transport function of the OmpC-Mla system, our observation here lends strong support to the notion that the Tol-Pal complex may be a major system for retrograde PL transport.

Discussion

Our work reveals that the Tol-Pal complex plays an important role in maintaining OM lipid homeostasis, possibly via retrograde PL transport. Removing the system causes accumulation of excess PLs (over LPS) in the OM (Figure 2). While pathways for anterograde PL transport remain to be discovered, this result indicates that PL flux to the OM may be intrinsically higher than that of LPS. Evidently, the ability to transport high levels of PLs to the OM allows cells to compensate for the loss of OMPs due to defects in assembly (Figure 2). Our data suggest that cells maintain an excess flux of PLs to the OM in order to offset changes in the unidirectional assembly pathways for other OM components, and then return the PL surplus to the IM via retrograde transport. Having bidirectional PL transport therefore provides a mechanism to regulate and ensure the formation of a stable OM.

It is not clear whether the Tol-Pal complex directly mediates retrograde PL transport. It is formally possible that the effects we have observed on retrograde PL transport are due to indirect effects of removing the Tol-Pal complex on other OM processes. However, we have already shown that removing this complex does not affect the assembly of both OMPs and LPS, two major components in the OM (Figure 1 - figure supplement 2). Consistently, we have demonstrated that strains with impaired OMP assembly do not have defects in retrograde PL transport (Figure 4A). We have also examined our strains under conditions where *tol-pal* mutants

247 do not exhibit apparent division defects (Gerding et al., 2007); it is thus unlikely that there could
248 be indirect effects on retrograde PL transport arising from the role of the Tol-Pal complex during
249 cell division. Therefore, we believe that the Tol-Pal complex may directly mediate PL transport.
250 One possibility is that this machine directly binds and transports lipids, although there are no
251 obvious lipid binding motifs or cavities found in available structures of the periplasmic
252 components (Deprez C et al., 2005; Carr et al., 2000). The Tol-Pal complex is related to the
253 ExbBD-TonB (Cascales et al., 2001; Celia et al., 2016), Agl-Glt (Faure et al., 2016), and Mot
254 (Cascales et al., 2001; Thormann and Paulick, 2010) systems, each of which uses pmf-energized
255 conformational changes to generate force for the uptake of metal-siderophores, for gliding
256 motility, or to power flagella rotation, respectively. In addition, both the Tol-Pal and ExbBD-
257 TonB complexes are hijacked by toxins (such as colicins) and bacteriophages to penetrate the
258 OM (Cascales et al., 2007). It is therefore also possible that the Tol-Pal complex acts simply as a
259 force generator to transport other PL-binding proteins across the periplasm, or perhaps bring the
260 OM close enough to the IM for PL transfer to occur via hemifusion events. For the latter
261 scenario, one can envision energized TolA pulling the OM inwards via its interaction with Pal,
262 which is anchored to the inner leaflet of the OM (Godlewska et al., 2009). While it remains
263 controversial, the formation of such "zones of adhesion", or membrane contact sites, has
264 previously been proposed (Bayer, 1991), and in fact, was suggested to be a mechanism for
265 retrograde transport of native and foreign lipids (Jones and Osborn, 1977).

266 That the Tol-Pal complex is involved in retrograde PL transport also has significant
267 implications for Gram-negative bacterial cell division. As part of the divisome, this system is
268 important for proper OM invagination during septum constriction (Gerding et al., 2007; Yeh et
269 al., 2010; Jacquier et al., 2015). How OM invagination occurs is unclear. Apart from physically
270 tethering the IM and the OM, we propose that removal of PLs from the inner leaflet of the OM,

possibly by the Tol-Pal complex, serves to locally reduce the surface area of the inner leaflet relative to the outer leaflet (McMahon and Gallop, 2005). According to the bilayer-couple model (Sheetz and Singer, 1974), this may then induce the requisite negative curvature in the OM at the constriction site, thus promoting formation of the new cell poles.

Given the importance of the Tol-Pal complex in OM stability and bacterial cell division, it would be an attractive target for small molecule inhibition. This is especially so in some organisms, including the opportunistic human pathogen *Pseudomonas aeruginosa*, where the complex is essential for growth (Dennis et al., 1996; Lo Sciuto et al., 2014). The lack of understanding of the true function of the Tol-Pal complex, however, has impeded progress. We believe that our work in elucidating a physiological role of this complex will accelerate efforts in this direction, and contribute towards the development of new antibiotics in our ongoing fight against recalcitrant Gram-negative infections.

Materials and Methods

Bacterial strains and growth conditions

All the strains used in this study are listed in Supplementary file 1A. *Escherichia coli* strain MC4100 [F^- *araD139* Δ*(argF-lac) U169 rpsL150 relA1 flbB5301 ptsF25 deoC1 ptsF25 thi*] (Casadaban, 1976) was used as the wild-type (WT) strain for most of the experiments. To achieve accumulation of phosphatidylserine (PS) in cells, a temperature-sensitive phosphatidylserine decarboxylase mutant (*psd2*), which accumulates PS at the non-permissive temperature, was used (Hawrot and Kennedy, 1978). NR754, an $araD^+$ revertant of MC4100 (Ruiz et al., 2008), was used as the WT strain for experiments involving overexpression of *lpxC* from the arabinose-inducible promoter (P_{BAD}). Δ*tolQ*, Δ*tolA* and Δ*tol-pal* deletions were

295 constructed using recombineering (Datsenko and Wanner, 2000) and all other gene deletion
296 strains were obtained from the Keio collection (Baba et al., 2006). Whenever needed, the
297 antibiotic resistance cassettes were flipped out as described (Datsenko and Wanner, 2000). Gene
298 deletion cassettes were transduced into relevant genetic background strains via P1 transduction
299 (Silhavy et al., 1984). Luria-Bertani (LB) broth (1% tryptone and 0.5% yeast extract,
300 supplemented with 1% NaCl) and agar were prepared as previously described (Silhavy et al.,
301 1984). Strains were grown in LB medium with shaking at 220 rpm at either 30˚C, 37˚C, or 42˚C,
302 as indicated. When appropriate, kanamycin (Kan; 25 μg ml^{-1}), chloramphenicol (Cam; 30 μg ml^{-}
303 ^{1}) and ampicillin (Amp; 125 μg ml^{-1}) were added.
304
305

306 Plasmid construction

307 All the plasmids used in this study are listed in Supplementary file 1B. Desired genes were
308 amplified from MC4100 chromosomal DNA using the indicated primers (sequences in
309 Supplementary file 1C). Amplified products were digested with indicated restriction enzymes
310 (New England Biolabs), which were also used to digest the carrying vector. After ligation,
311 recombinant plasmids were transformed into competent NovaBlue (Novagen) cells and selected
312 on LB plates containing appropriate antibiotics. DNA sequencing (Axil Scientific, Singapore)
313 was used to verify the sequence of the cloned gene.

314 To generate $tolR_{D23R}$ mutant construct, site-directed mutagenesis was conducted using
315 relevant primers listed in Supplementary file 1C with pET23/42*tolR* as the initial template.
316 Briefly, the entire template was amplified by PCR and the resulting PCR product mixture
317 digested with DpnI for > 1 h at 37˚C. Competent NovaBlue cells were transformed with 1 µl of
318 the digested PCR product and plated onto LB plates containing ampicillin. DNA sequencing
319 (Axil Scientific, Singapore) was used to verify the introduction of the desired mutation.

320

321 Analysis of [^{32}P]-labelled lipid A

322 Mild acid hydrolysis was used to isolate lipid A as previously described (Zhou et al.,
323 1999) with some modifications. 5-ml cultures were grown in LB broth (inoculated from an
324 overnight culture at 1:100 dilution) containing [^{32}P]-disodium phosphate (final 1 µCi ml^{-1}; Perkin
325 Elmer product no. NEX011001MC) till mid-log phase (OD600 ~0.5 - 0.7). One MC4100 WT
326 culture labelled with [^{32}P] was treated with EDTA (25 mM pH 8.0) for 10 min prior to
327 harvesting. Cells were harvested at 4,700 x *g* for 10 min, washed twice with 1 ml PBS (137 mM
328 NaCl, 2.7 mM KCl, 10 mM Na_2HPO_4, 1.8 mM KH_2PO_4, pH 7.4) and suspended in PBS (0.32
329 ml) again. Chloroform (0.4 ml) and methanol (0.8 ml) were added and the mixtures were

330 incubated at room temperature for 20 min with slow shaking (60 rpm) to make the one-phase
331 Bligh-Dyer mixture (chloroform:methanol:water = 1:2:0.8). Mixtures were then centrifuged at
332 21,000 x *g* for 30 min. Pellets obtained were washed once with fresh one-phase Bligh-Dyer
333 system (1 ml) and centrifuged as above. Resulting pellets were suspended in 0.45 ml of sodium
334 acetate (12.5 mM, pH 4.5) containing SDS (1 %) and heated at 100˚C for 30 min. After cooling
335 to room temperature, chloroform and methanol (0.5 ml each) were added to create a two-phase
336 Bligh-Dyer mixture (chloroform:methanol:water = 2:2:1.8). The lower (organic) phase of each
337 mixture was collected after phase partitioning via centrifugation at 21,000 x *g* for 30 min. This
338 was washed once with upper phase (0.5 ml) of freshly prepared two-phase Bligh-Dyer mixture
339 and centrifuged as above. Finally, all the collected lower phases containing [^{32}P]-labelled lipid A
340 were air-dried overnight. Dried radiolabelled lipid A samples were suspended in 50 µl of
341 chloroform:methanol (2:1) and equal amounts (~1,000 cpm) of radioactivity were spotted on
342 silica-gel coated TLC (Thin Layer Chromatography) plates (Merck). TLCs were developed in
343 chambers pre-equilibrated overnight with solvent system chloroform:pyridine:98 % formic
344 acid:water (50:50:14.6:5). TLC plates were air-dried overnight and later visualized by phosphor
345 imaging (STORM, GE healthcare). The densitometric analysis of the spots obtained on the
346 phosphor images of TLCs was carried out using ImageQuant TL analysis software (version 7.0,
347 GE Healthcare). Average levels of hepta-acylated lipid A (expressed as a percentage of total
348 lipid A in each sample) were obtained from three independent experiments.
349
350
351
352 <u>Sucrose density gradient fractionation</u>

353 Sucrose density gradient centrifugation was performed as previously described (Chng et
354 al., 2010) with some modifications. For each strain, a 10/50-ml culture (inoculated from an
355 overnight culture at 1:100 dilution) was grown in LB broth until OD_{600} reached ~0.5 – 0.7. For
356 radiolabeling, indicated radioisotopes were added from the start of inoculation. Cells were
357 harvested by centrifugation at 4,700 x *g* for 10 min, suspended to wash once in 5 ml of cold
358 Buffer A (Tris-HCl, 10 mM pH 8.0), and centrifuged as above. Cells were resuspended in 6 ml
359 of Buffer B (Tris-HCl, 10 mM pH 8.0 containing 20% sucrose (w/w), 1 mM PMSF and 50 μg ml
360 $^{-1}$ DNase I), and lysed by a single passage through a high pressure French press (French Press G-
361 M, Glen Mills) homogenizer at 8,000 psi. Under these conditions, lipid mixing between inner
362 and outer membranes is minimal (Chng et al., 2010). Unbroken cells were removed by
363 centrifugation at 4,700 x *g* for 10 min. The cell lysate was collected, and 5.5 ml of cell lysate was
364 layered on top of a two-step sucrose gradient consisting of 40% sucrose solution (5 ml) layered
365 on top of 65% sucrose solution (1.5 ml) at the bottom of the tube. All sucrose (w/w) solutions
366 were prepared in Buffer A. Samples were centrifuged at 39,000 rpm for 16 h in a Beckman
367 SW41 rotor in an ultracentrifuge (Model XL-90, Beckman). 0.8-ml fractions (usually 15
368 fractions) were manually collected from the top of each tube.
369
370 Analysis of OMP and LPS levels in isolated OMs
371 OM fragments were isolated from 50 ml of cells following growth, cell lysis and
372 application of sucrose density gradient fractionation, as described above. Instead of manual
373 fractionation, OM fragments (~1 ml) were isolated from the 40%/65% sucrose solution interface
374 by puncturing the side of the tube with a syringe. Buffer A (1 ml) was added to the OM
375 fragments to lower the sucrose concentration and reduce viscosity. The OM fragments were then
376 pelleted in a microcentrifuge at 21,000 x *g* for 30 min and then resuspended in 200 - 250 μl

377 Buffer A. Protein concentrations of these OM preparations were determined using Bio-Rad D_C
378 protein assay. The same amount of OM (based on protein content) for each strain was analyzed
379 by reducing SDS-PAGE and immunoblotted using antibodies directed against OmpC, OmpF,
380 LamB, BamA, LptE and LPS. For LPS quantification, five-fold serial dilutions of WT OMs were
381 ran alongside the other OM samples as standards. Densitometric analysis of the LPS bands was
382 carried out using ImageJ analysis software, and calibrated using ratio standard curves generated
383 from the serial dilution standards (Pitre et al., 2007). LPS levels found in the OMs of indicated
384 strains were normalized to WT. This quantification was performed three times for the same
385 samples, and the average data was plotted.
386
387 Analysis of steady-state [^{3}H]-glycerol-labelled PL distribution in IMs and OMs
388 To specifically label cellular PLs, 10-ml cells were grown at 37˚C in LB broth
389 (inoculated from an overnight culture at 1:100 dilution) containing [2-^{3}H]-glycerol (final 1 μCi
390 ml^{-1}; Perkin Elmer product no. NET022L001MC) until OD_{600} reached ~0.5 - 0.7. Once the
391 desired OD_{600} was achieved, cultures were immediately mixed with ice-cold Buffer A containing
392 CCCP (50 μM) to stop the labeling of the cultures. Cells were pelleted, lysed, and fractionated
393 on sucrose density gradients, as described above. 0.8-ml fractions were collected from each tube,
394 as described above, and 300 μl from each fraction was mixed with 2 ml of Ultima Gold
395 scintillation fluid (Perkin Elmer, Singapore). Radioactivity ([^{3}H]-count) was measured on a
396 scintillation counter (MicroBeta$^{2®}$, Perkin-Elmer). Based on [^{3}H]-profiles, IM and OM peaks
397 were identified and peak areas determined after background subtraction (average count of first 5
398 fractions was taken as background). For each strain, relative [^{3}H]-PL levels in the IM and OM
399 were expressed as a percentage of the sum in both membranes (see Figure 2A upper panel). The
400 average percent [^{3}H]-PL in the OM for each strain (obtained from three independent

401 experiments) was then compared to that for the WT strain to calculate fold changes (see Figure
402 2A lower panel).
403
404 Determination of PL/LPS ratios in [^{14}C]-acetate labelled OMs (see Fig. S5 for workflow and
405 results)
406 To specifically label all cellular lipids (including LPS), 10-ml cells were grown at 37˚C
407 in LB broth (inoculated from an overnight culture at 1:100 dilution) containing [1-^{14}C]-acetate
408 (final 0.2 μCi ml^{-1}; Perkin Elmer product no. NEC084A001MC) until OD_{600} reached ~0.5 – 0.7.
409 At this OD, cultures were transferred immediately to ice-cold Buffer A (5 ml), pelleted, lysed,
410 and fractionated on sucrose density gradients, as described above. 0.8-ml fractions were
411 collected from each tube, as described above, and 50 μl from each fraction was mixed with 2 ml
412 of Ultima Gold scintillation fluid (Perkin Elmer, Singapore). Based on [^{14}C]-profiles, IM and
413 OM peaks were identified. OM fractions were then pooled, and treated as outlined below to
414 differentially extract PLs and LPS for relative quantification within each OM pool. For each
415 strain, the whole experiment was conducted and the OM PL/LPS ratio obtained three times.
416 Each OM pool (0.32 ml) was mixed with chloroform (0.4 ml) and methanol (0.8 ml) to
417 make a one-phase Bligh-Dyer mixture (chloroform:methanol:water = 1:2:0.8). The mixtures
418 were vortexed for 2 min and later incubated at room temperature for 20 min with slow shaking at
419 60 rpm. After centrifugation at 21,000 x *g* for 30 min, the supernatants (S1) were collected. The
420 resulting pellets (P1) were washed once with fresh 0.95 ml one-phase Bligh-Dyer solution and
421 centrifuged as above. The insoluble pellets (P2) were air dried and used for LPS quantification
422 (see below). The supernatants obtained in this step (S2) were combined with S1 to get the
423 combined supernatants (S3), which contained radiolabelled PLs. To these, chloroform (0.65 ml)
424 and methanol (0.65 ml) were added to convert them to two-phase Bligh-Dyer mixtures

425 (chloroform:methanol:water = 2:2:1.8). After a brief vortexing step, the mixtures were
426 centrifuged at 3000 x *g* for 10 min to separate the immiscible phases, and the lower organic
427 phases were collected. These were washed once with equal volumes of water and centrifuged as
428 above, and the lower organic phases (containing radiolabelled PLs) recollected and air dried.
429 Finally, the dried PLs were dissolved in 50 µl of a mixture of chloroform:methanol (2:1). Equal
430 volumes (20 µl) of PL solutions were mixed with 2 ml of Ultima Gold scintillation fluid (Perkin
431 Elmer, Singapore). The [^{14}C]-counts were measured using scintillation counting (MicroBeta$^{2®}$,
432 Perkin-Elmer) and taken as the levels of PLs isolated from the OMs.

433 To quantify LPS, the P2 pellets were suspended in 2X reducing SDS-PAGE loading
434 buffer (40 µl) and boiled for 10 min. Equal volumes (15 µl) were loaded and subjected to SDS-
435 PAGE (15% Tris.HCl). Gels were air-dried between porous films (Invitrogen) and exposed to
436 the same phosphor screen along with standards (GE healthcare). To generate a standard curve for
437 LPS quantification, the WT OM pellet sample was serially diluted two-fold and equal volumes
438 of diluted samples were resolved on SDS-PAGE and dried as above. The densitometric analysis
439 of bands (i.e. LPS from each OM) was carried out using ImageQuant TL analysis software
440 (version 7.0, GE Healthcare). To allow proper comparison and quantification, the LPS gels from
441 triplicate experiments were exposed on the same phosphor screen along with the standards (see
442 Figure 2 - figure supplement 3).

443 For each strain, the arbitrary PL/LPS ratio in the OM was obtained by taking the levels of
444 PLs (represented by [^{14}C]-counts of PL fraction) divided by the LPS levels (represented by gel
445 band density), averaged across three independent replicates (see Figure 2 - figure supplement 3C
446 and Figure 2B upper panel). The average PL/LPS ratio in the OM for each strain was then
447 compared to that for the WT strain to calculate fold changes (see Figure 2B lower panel).

448

449 Quantification of OM vesiculation

450 For each strain, 10-ml cells were grown at 37˚C in LB broth (inoculated from an
451 overnight culture at 1:100 dilution) containing [1-^{14}C]-acetate (final 0.2 μCi ml^{-1}; Perkin Elmer
452 product no. NEC084A001MC) until OD_{600} reached ~0.7. At this OD, cultures were harvested to
453 obtain the cell pellets, and supernatants containing OM vesicles. Cell pellets were washed twice
454 with Buffer A and finally suspended in the same buffer (0.2 ml). To obtain OM vesicles,
455 supernatants were filtered through 0.45 μm filters followed by ultracentrifugation in a SW41.Ti
456 rotor at 39,000 rpm for 1 h. Finally, the OM vesicles in the resulting pellets were washed and re-
457 suspended in 0.2 ml of Buffer A. Radioactive counts in cell pellets and OM vesicles were
458 measured after mixing with 2 ml of Ultima Gold scintillation fluid (Perkin Elmer, Singapore).
459 Radioactivity ([^{14}C]-count) was measured on a scintillation counter (MicroBeta$^{2®}$, Perkin-
460 Elmer).

461

462 PG/CL turnover assay (pulse-chase and single time-point (2-h) analysis)

463 PG/CL turnover pulse-chase experiments were performed using the *psd2* background,
464 which accumulated PS and PG/CL during growth at restrictive temperature. For each strain, cells
465 were grown in 70 ml LB broth (inoculated from an overnight culture at 1:100 dilution) at the
466 permissive temperature (30˚C) until OD_{600} reached ~0.15 - 0.2. The culture was then shifted for
467 4 h at the restrictive temperature (42˚C) and labelled with [^{32}P]-disodium phosphate (final 1 μCi
468 ml^{-1}) during the last 30 min at the restrictive temperature (42˚C). After labeling, cells were
469 harvested by centrifugation at 4,700 x *g* for 10 min, washed once with cold LB broth (10 ml) and
470 centrifuged again at 4,700 x *g* for 10 min. Cells were then resuspended in fresh LB broth (70 ml)
471 and the chase was started in the presence of non-radioactive disodium phosphate (1000-fold
472 molar excess) at either the permissive temperature, with or without addition of carbonyl cyanide

473 *m*-chlorophenyl hydrazone (CCCP; 50 μM), or at the restrictive temperature in the presence of
474 hydroxylamine (HA; 10 mM). At the start (0 min) and different times (15, 30, 45, 90 and 120
475 min) during the chase, a portion of the culture (either 15 ml or 10 ml) was collected and mixed
476 immediately with equal volume of ice-cold Buffer A containing CCCP (50 μM) and
477 hydroxylamine (10 mM). Cells were harvested by centrifugation at 4,700 x *g* for 10 min and then
478 resuspended in 6 ml of Buffer B containing CCCP (50 μM) and hydroxylamine (10 mM). Cells
479 were lysed, and fractionated on sucrose density gradients, as described above. 0.8-ml fractions
480 were collected from each tube, as described above. Fractions 7-9 and 12-14 contained the IM and
481 OM fractions, respectively. To extract PLs from the IM and OM pools (2.4 ml), methanol (6 ml)
482 and chloroform (3 ml) were added to make one-phase Bligh-Dyer mixtures. These were
483 incubated at room temperature for 60 min with intermittent vortexing. Chloroform (3 ml) and
484 sterile water (3 ml) were then added to generate two-phase Bligh-Dyer mixtures. After brief
485 vortexing, the lower organic phases were separated from the top aqueous phases by
486 centrifugation at 3,000 x *g* for 10 min. These were washed once with equal volumes of water and
487 centrifuged as above, and the lower organic phases (containing radiolabelled PLs) recollected
488 and air dried. Finally, the dried PLs were dissolved in 40 μl of a mixture of chloroform:methanol
489 (2:1) and spotted onto silica-gel coated TLC plates (Merck). Equal amounts (in cpm) of
490 radioactivity were spotted for each sample. TLCs were developed in pre-equilibrated chambers
491 containing solvent system chloroform:methanol:water (65:25:4). TLC plates were dried, and
492 visualized by phosphor imaging (STORM, GE healthcare). Densitometric analysis of the PL
493 spots on the phosphor image of TLCs was conducted using the ImageQuant TL analysis software
494 (version 7.0, GE Healthcare). The levels of each major PL species were expressed as a
495 percentage of all detected PL species (essentially the whole lane), and plotted against time (see
496 Figures 3 and Figure 3 - figure supplement 1).

497 For single time-point analysis, 30-ml cultures were grown and labelled with [^{32}P]-
498 disodium phosphate (final 1 μCi ml^{-1}) at the restrictive temperature. For strains harboring
499 plasmids used for overexpressing OmpC-Mla components, arabinose (0.2 %) was added during
500 growth at the permissive as well as restrictive temperatures. After washing and resuspension in
501 fresh LB broth (30 ml), the chase was started in the presence of non-radioactive disodium
502 phosphate (1000-fold molar excess) at the permissive temperature. At start (0 h) and 2 h during
503 the chase, a portion of the culture (15 and 10 ml) was collected and processed similarly as pulse
504 chase analysis described above. The levels of PG/CL in the membranes at each time point were
505 expressed as a percentage of the sum of PE, PS and PG/CL. For each strain, IM and OM PG/CL
506 turnover were expressed as the difference between percentage PG/CL levels at 0-h and 2-h time
507 points divided by that at 0-h. Average PG/CL turnover values were obtained from three
508 independent experiments conducted (see Figure 4 and Figure 4 - figure supplement 1).
509
510

511 OM permeability assay

512 OM sensitivity against SDS/EDTA was judged by colony-forming unit (cfu) analyses on
513 LB agar plates containing indicated concentrations of SDS/EDTA. Briefly, 5-ml cultures were
514 grown (inoculated with overnight cultures at 1:100 dilution) in LB broth at 37˚C until OD_{600}
515 reached ~1.0. Cells were normalized according to OD_{600}, first diluted to OD_{600} = 0.1 (~10^8 cells),
516 and then serial diluted in LB with seven 10-fold dilutions using 96-well microtiter plates
517 (Corning). Two microliters of the diluted cultures were manually spotted onto the plates and
518 incubated overnight at 37˚C.

519

520 LpxC overexpression (growth curves and viability assay)

521 For each strain, a 10-ml culture was inoculated in LB broth supplemented with arabinose
522 (0.2 %) from the overnight culture to make the initial OD_{600} of 0.05. Cells were grown at 37˚C
523 and the OD_{600} of the cultures was measured hourly. At the start of growth (0 h) and at 4 and 7 h
524 during growth, 100 µl of cells were collected and then serial diluted in LB/cam with six 10-fold
525 dilutions using 96-well microtiter plates (Corning). Five microliters of the non-diluted and
526 diluted cultures were manually spotted on LB/cam agar plates (no arabinose). Plates were
527 incubated overnight at 37˚C.

528

529 IM (NADH activity) and OM marker (LPS) analysis during sucrose gradient fractionation

530 The inner membrane enzyme, NADH oxidase, was used as a marker for the IM; its
531 activity was measured as previously described (56). Briefly, 30 µl of each fraction from the
532 sucrose density gradient was diluted 4-fold with 20 mM Tris.HCl, pH 8.0 in a 96-well format
533 and 120 µl of 100 mM Tris.HCl, pH 8.0 containing 0.64 mM NADH (Sigma) and 0.4 mM
534 dithiothreitol (DTT, Sigma) was added. Changes in fluorescence over time due to changes in

535 NADH (λex = 340 nm, λem = 465 nm) concentration was monitored using a plate reader (Perkin
536 Elmer). The activity of NADH oxidase in pooled IM and OM fractions relative to the sum of
537 these fractions was determined.

538 LPS was used as a marker for the OM and detected using LPS dot blots. OM fractions
539 were pooled together and 2 µl of the fractions were spotted on nitrocellulose membranes (Bio-
540 Rad). Spotted membranes were allowed to dry at room temperature for 1 h and then the
541 membranes were probed with antibodies against LPS.

542

543 SDS-PAGE and immunoblotting

544 All samples subjected to SDS-PAGE were mixed with 2X Laemmli reducing buffer and
545 boiled for 10 min at 100˚C. Equal volumes of the samples were loaded onto the gels. Unless
546 otherwise stated, SDS-PAGE was performed according to Laemmli using the 12% or 15%
547 Tris.HCl gels (Laemmli, 1970). Immunoblotting was performed by transferring protein bands
548 from the gels onto polyvinylidene fluoride (PVDF) membranes (Immun-Blot® 0.2 µm, Bio-Rad)
549 using the semi-dry electroblotting system (Trans-Blot® TurboTM Transfer System, Bio-Rad).
550 Membranes were blocked using 1X casein blocking buffer (Sigma). Mouse monoclonal α-OmpC
551 antibody was a gift from Swaine Chen and used at a dilution of 1:5,000 (Khetrapal et al., 2015).
552 Rabbit α-LptE (from Daniel Kahne) (Chng et al., 2010) and α-OmpF antisera (Rajeev Misra)
553 (Charlson et al., 2006) were used at 1:5,000 dilutions. Rabbit α-BamA antisera (from Daniel
554 Kahne) was used at 1:40,000 dilution. Rabbit α-LpxC antisera (generous gift from Franz
555 Narberhaus) was used at 1:5,000 dilution. Mouse monoclonal α-LPS antibody (against LPS-core)
556 was purchased from Hycult biotechnology and used at 1:5,000 dilutions. Rabbit polyclonal α-
557 LamB antibodies was purchased from Bioss (USA) and used at 1:1,000 dilution. α-mouse IgG
558 secondary antibody conjugated to HRP (from sheep) and α-rabbit IgG secondary antibody

559 conjugated to HRP (from donkey) were purchased from GE Healthcare and used at 1:5,000
560 dilutions. Luminata Forte Western HRP Substrate (Merck Milipore) was used to develop the
561 membranes and chemiluminescent signals were visualized by G:BOX Chemi XT 4 (Genesys
562 version1.3.4.0, Syngene).
563

Acknowledgments

We thank Zhi-Soon Chong for constructing the Δ*mlaC* allele, and Chee-Geng Chia for performing preliminary experiments. We are grateful to Swaine Chen (NUS), Rajeev Misra (Arizona State U), Daniel Kahne (Harvard U) and Franz Narberhous (RUHR Universitat Bochum) for their generous gifts of α-OmpC, α-OmpF, α-LptE and α-BamA, and α-LpxC antibodies, respectively. Finally, we thank William F. Burkholder (Institute of Molecular and Cell Biology) and Jean-Francois Collet (U Catholique de Louvain) for critical comments and suggestions on the manuscript. This work was supported by the National University of Singapore Start-up funding, the Singapore Ministry of Education Academic Research Fund Tier 1 and Tier 2 (MOE2013-T2-1-148) grants, and the Singapore Ministry of Health National Medical Research Council under its Cooperative Basic Research Grant (NMRC/CBRG/0072/2014) (all to S.-S.C.).

References

Baba T, et al. (2006) Construction of *Escherichia coli* K-12 in-frame, single-gene knockout mutants: the Keio collection. *Mol Syst Biol* 2:2006.0008.

Bayer ME (1991) Zones of membrane adhesion in the cryofixed envelope of *Escherichia coli*. *J Struct Biol* 107(3):268-280.

Bernadac A, Gavioli M, Lazzaroni JC, Raina S, Lloubes R (1998) *Escherichia coli tol-pal* mutants form outer membrane vesicles. *J Bacteriol* 180(18):4872-4878.

Bernstein A, Rolfe B, Onodera K (1972) Pleiotropic properties and genetic organization of the *tolA, B* locus of *Escherichia coli* K-12. *J Bacteriol* 112(1):74-83.

Bishop RE (2005) The lipid A palmitoyltransferase PagP: molecular mechanisms and role in bacterial pathogenesis. *Mol Microbiol* 57(4):900-912.

Carr S, Penfold CN, Bamford V, James R, Hemmings AM (2000) The structure of TolB, an essential component of the *tol*-dependent translocation system, and its protein-protein interaction with the translocation domain of colicin E9. *Structure* 8(1):57-66.

Casadaban MJ (1976) Transposition and fusion of the *lac* genes to selected promoters in *Escherichia coli* using bacteriophage lambda and Mu. *J Mol Biol* 104(3):541-555.

Cascales E, Gavioli M, Sturgis JN, Lloubes R (2000) Proton motive force drives the interaction of the inner membrane TolA and outer membrane Pal proteins in *Escherichia coli*. *Mol Microbiol* 38(4):904-915.

Cascales E, Lloubes R, Sturgis JN (2001) The TolQ-TolR proteins energize TolA and share homologies with the flagellar motor proteins MotA-MotB. *Mol Microbiol* 42(3):795-807.

Cascales E, et al. (2007) Colicin biology. *Microbiol Mol Biol Rev* 71(1):158-229.

Celia H, et al. (2016) Structural insight into the role of the Ton complex in energy transduction. *Nature* 538(7623):60-65.

600 Charlson ES, Werner JN, Misra R (2006) Differential effects of *yfgL* mutation on *Escherichia*
601 *coli* outer membrane proteins and lipopolysaccharide. *J Bacteriol* 188(20):7186-7194.
602 Chong ZS, Woo WF, Chng SS (2015) Osmoporin OmpC forms a complex with MlaA to
603 maintain outer membrane lipid asymmetry in *Escherichia coli*. *Mol Microbiol* 98(6):1133-
604 1146.
605 Chng SS, Gronenberg LS, Kahne D (2010) Proteins required for lipopolysaccharide transport in
606 *Escherichia coli* form a transenvelope complex. *Biochemistry* 49(22):4565-4567.
607 Clavel T, Lazzaroni JC, Vianney A, Portalier R (1996) Expression of the *tolQRA* genes of
608 *Escherichia coli* K-12 is controlled by the RcsC sensor protein involved in capsule synthesis.
609 *Mol Microbiol* 19(1):19-25.
610 Cronan JE (2003) Bacterial membrane lipids: where do we stand? *Annu Rev Microbiol* 57:203-
611 224.
612 Dalebroux ZD, Matamouros S, Whittington D, Bishop RE, Miller SI (2014) PhoPQ regulates
613 acidic glycerophospholipid content of the *Salmonella typhimurium* outer membrane. *Proc*
614 *Natl Acad Sci USA* 111(5):1963-1968.
615 Datsenko KA, Wanner BL (2000) One-step inactivation of chromosomal genes in *Escherichia*
616 *coli* K-12 using PCR products. *Proc Natl Acad Sci USA* 97(12):6640-6645.
617 Dennis JJ, Lafontaine ER, Sokol PA (1996) Identification and characterization of the *tolQRA*
618 genes of *Pseudomonas aeruginosa*. *J Bacteriol* 178(24):7059-7068.
619 Deprez C, et al. (2005) Solution structure of the *E. coli* TolA C-termical domain reveals
620 conformational changes upon binding to the phage g3p N-terminal domain. *J Mol Biol*
621 346(4):1047-1057.
622 Donohue-Rolfe AM, Schaechter M (1980) Translocation of phospholipids from the inner to the
623 outer membrane of *Escherichia coli*. *Proc Natl Acad Sci USA* 77(4):1867-1871.

624 Faure LM, et al. (2016) The mechanism of force transmission at bacterial focal adhesion
625 complexes. *Nature* 539(7630):530-535.
626 Fuhrer F, Langklotz S, Narberhaus F (2006) The C-terminal end of LpxC is required for
627 degradation by the FtsH protease. *Mol Microbiol* 59(3):1025-1036.
628 Gerding MA, Ogata Y, Pecora ND, Niki H, de Boer PAJ (2007) The trans-envelope Tol-Pal
629 complex is part of the cell division machinery and required for proper outer-membrane
630 invagination during cell constriction in *E. coli*. *Mol Microbiol* 63(4):1008-1025.
631 Germon P, Ray MC, Vianney A, Lazzaroni JC (2001) Energy-dependent conformational changes
632 in the TolA protein of *Escherichia coli* involves its N-terminal domain, TolQ, and TolR. *J*
633 *Bacteriol* 183(14):4110-4114.
634 Gresock MG, Kastead KA, Postle K (2015) From homodimer to heterodimer and back:
635 elucidating the TonB energy transduction cycle. *J Bacteriol* 197(21):3433-3445.
636 Godlewska R, Wisniewska K, Pietras Z, Jagusztyn-Krynicka EK (2009) Peptidoglycan-
637 associated lipoprotein (Pal) of Gram-negative bacteria: function, structure, role in
638 pathogenesis and potential application in immunoprophylaxis. *FEMS Microbiol Lett* 298(1):1-
639 11.
640 Gully D, Bouveret E (2006) A protein network for phospholipid synthesis uncovered by a variant
641 of the tandem affinity purification method in *Escherichia coli*. *Proteomics* 6:282-293.
642 Guzman LM, Belin D, Carson MJ, Beckwith J (1995) Tight regulation, modulation, and high-
643 level expression by vectors containing the arabinose P_{BAD} promoter. *J Bacteriol*
644 177(14):4121-4130.
645 Hagan CL, Silhavy TJ, Kahne D (2011) β-barrel membrane protein assembly by the Bam
646 complex. *Annu Rev Biochem* 80:189-210.

647 Hawrot E, Kennedy EP (1978) Phospholipid composition and membrane function in
648 phosphatidylserine decarboxylase mutants of *Escherichia coli*. *J Biol Chem* 253(22):8213-
649 8220.
650 Jacquier N, Frandi A, Viollier PH, Greub G (2015) Disassembly of a medial transenvelope
651 structure by antibiotics during intracellular division. *Chem Biol* 22(9):1217-1227.
652 Jones NC, Osborn MJ (1977) Translocation of phospholipids between the outer and inner
653 membranes of *Salmonella typhimurium*. *J Biol Chem* 252(20):7405-7412.
654 Kanemasa Y, Akamatsu Y, Nojima S (1967) Composition and turnover of the phospholipids in
655 *Escherichia coli*. *Biochim Biophys Acta* 144(2):382-390.
656 Kanfer J, Kennedy EP (1963) Metabolism and function of bacterial lipids I. Metabolism of
657 phospholipids in *Escherichia coli* B. *J Biol Chem* 238(9):2919-2922.
658 Khetrapal V, et al. (2015) A set of powerful negative selection systems for unmodified
659 Enterobacteriaceae. *Nucleic Acids Res* 43:e83.
660 Laemmli UK (1970) Cleavage of structural proteins during the assembly of the head of
661 bacteriophage T4. *Nature* 227(5259):680-685.
662 Langley KE, Hawrot E, Kennedy EP (1982) Membrane assembly: movement of
663 phosphatidylserine between the cytoplasmic and outer membranes of *Escherichia coli*. *J*
664 *Bacteriol* 152(3):1033-1041.
665 Lazzaroni JC, Portalier RC (1981) Genetic and biochemical characterization of periplasmic-
666 leaky mutants of *Escherichia coli* K-12. *J Bacteriol* 145(3):1351-1358.
667 Lloubes R, et al. (2001) The Tol-Pal proteins of the *Escherichia coli* cell envelope: an energized
668 system required for outer membrane integrity? *Res Microbiol* 152(6):523-529.
669 Lo Sciuto A, et al. (2014) The periplasmic protein TolB as a potential drug target in
670 *Pseudomonas aeruginosa*. *PLoS One* 9:e103784.

671 Malinverni JC, Silhavy TJ (2009) An ABC transport system that maintains lipid asymmetry in
672 the Gram-negative outer membrane. *Proc Natl Acad Sci USA* 106(19):8009-8014.
673 McMahon HT, Gallop JL (2005) Membrane curvature and mechanisms of dynamic cell
674 membrane remodelling. *Nature* 438(7068):590-596.
675 Nikaido H (2003) Molecular basis of bacterial outer membrane permeability revisited. *Microbiol*
676 *Mol Biol Rev* 67(4):593-656.
677 Okuda S, Sherman DJ, Silhavy TJ, Ruiz N, Kahne D (2016) Lipopolysaccharide transport and
678 assembly at the outer membrane: the PEZ model. *Nat Rev Microbiol* 14:337-345.
679 Okuda S, Tokuda H (2011) Lipoprotein sorting in bacteria. *Annu Rev Microbiol* 65:239-259.
680 Pitre A, Pan Y, Pruett S, Skalli O (2007) On the use of ratio standard curves to accurately
681 quantitate relative changes in protein levels by western blot. *Anal Biochem* 361(2):305-307.
682 Ruiz N, Chng SS, Hinikera A, Kahne D, Silhavy TJ (2010) Nonconsecutive disulphide bond
683 formation in an essential integral outer membrane protein. *Proc Natl Acad Sci USA*
684 107(27):12245-12250.
685 Ruiz N, Falcone B, Kahne D, Silhavy TJ (2005) Chemical conditionality: a genetic strategy to
686 probe organelle assembly. *Cell* 121:307-317.
687 Ruiz N, Gronenberg LS, Kahne D, Silhavy TJ (2008) Identification of two inner-membrane
688 proteins required for the transport of lipopolysaccharide to the outer membrane of *Escherichia*
689 *coli*. *Proc Natl Acad Sci USA* 105(14):5537-5542.
690 Satre M, Kennedy EP (1978) Identification of bound pyruvate essential for the activity of
691 phosphatidylserine decarboxylase of *Escherichia coli*. *J Biol Chem* 253(2):479-483.
692 Sheetz MP, Singer SJ (1974) Biological membranes as bilayer couples. A molecular mechanism
693 of drug-erythrocyte interactions. *Proc Natl Acad Sci USA* 71(11):4457-4461.

694 Silhavy TJ, Berman ML, Enquist LW (1984) *Experiments with Gene fusions* (Cold Spring
695 Harbor Laboratory Press, Cold Spring Harbor, New York).
696 Sturgis JN (2001) Organisation and evolution of the *tol-pal* gene cluster. *J Mol Microbiol*
697 *Biotechnol* 3(1):113-122.
698 Thong S, et al. (2016) Defining key roles for auxillary proteins in an ABC transporter that
699 maintains bacterial outer membrane lipid asymmetry. *eLife* 5:e19042.
700 Thormann KM, Paulick A (2010) Tuning the flagellar motor. *Microbiology* 156(Pt 5):1275-
701 1283.
702 Vines ED, Marolda CL, Balachandran A, Valvano MA (2005) Defective O-antigen
703 polymerization in *tolA* and *pal* mutants of *Escherichia coli* in response to extracytoplasmic
704 stress. *J Bacteriol* 187(10):3359-3368.
705 Walburger A, Lazdunski C, Corda Y (2002) The Tol/Pal system function requires an interaction
706 between the C-terminal domain of TolA and the N-terminal domain of TolB. *Mol Microbiol*
707 44(3):695-708.
708 Witty M, et al. (2002) Structure of the periplasmic domain of *Pseudomonas aeruginosa* TolA:
709 evidence for an evolutionary relationship with the TonB transporter protein. *EMBO J*
710 21(16):4207-4218.
711 Wu T, et al. (2005) Identification of a multicomponent complex required for outer membrane
712 biogenesis in *Escherichia coli*. *Cell* 121:235-245.
713 Wu T, et al. (2006) Identification of a protein complex that assembles lipopolysaccharide in the
714 outer membrane of *Escherichia coli*. *Proc Natl Acad Sci USA* 103(31):11754-11759.
715 Yeh YC, Comolli LR, Downing KH, Shapiro L, McAdams HH (2010) The *Caulobacter* Tol-Pal
716 complex is essential for outer membrane integrity and the positioning of a polar localization
717 factor. *J Bacteriol* 192(19):4847-4858.

718 Yem DW, Wu HC (1978) Physiological characterization of an *Escherichia coli* mutant altered in
719 the structure of murein lipoprotein. *J Bacteriol* 133(3):1419-1426.
720 Yokoto K, Kito M (1982) Transfer of the phosphatidyl moiety of phosphatidylglycerol to
721 phosphatidylethanolamine in *Escherichia coli*. *J Bacteriol* 151(2):952-961.
722 Zhou Z, Lin S, Cotter RJ, Raetz CRH (1999) Lipid A modifications characteristic of *Salmonella*
723 *typhimurium* are induced by NH_4VO_3 in *Escherichia coli* K-12. *J Biol Chem* 274(26):18503-
724 18514.

725

Figures

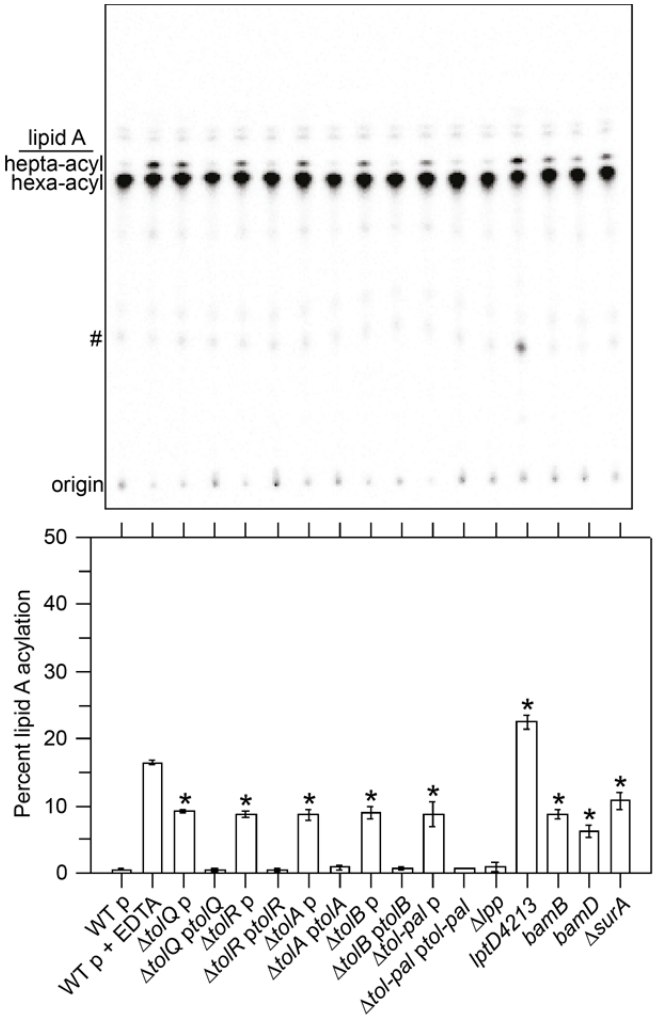

Figure 1 Cells lacking the Tol-Pal complex accumulate PLs in the outer leaflet of the OM as judged by lipid A acylation. Thin layer chromatographic (TLC) analysis of [^{32}P]-labelled lipid A extracted from WT, Δ*tol-pal*, and various mutant strains (*see text*). Where indicated, WT and *tol-pal* mutants contain an empty pET23/42 plasmid (p) (Wu et al., 2006) or one expressing the corresponding *tol-pal* gene(s) at low levels (e.g. p*tol-pal*). As a positive control for lipid A acylation, WT cells were treated with EDTA (to chelate Mg^{2+} and destabilize the LPS layer) prior to extraction. Equal amounts of radioactivity were spotted for each sample. Lipid spots annotated # represent 1-pyrophosphoryl-lipid A. Average percentages of lipid A acylation and

736 standard deviations were quantified from triplicate experiments and plotted below. Student's t-

737 tests: * $p < 0.005$ as compared to WT.

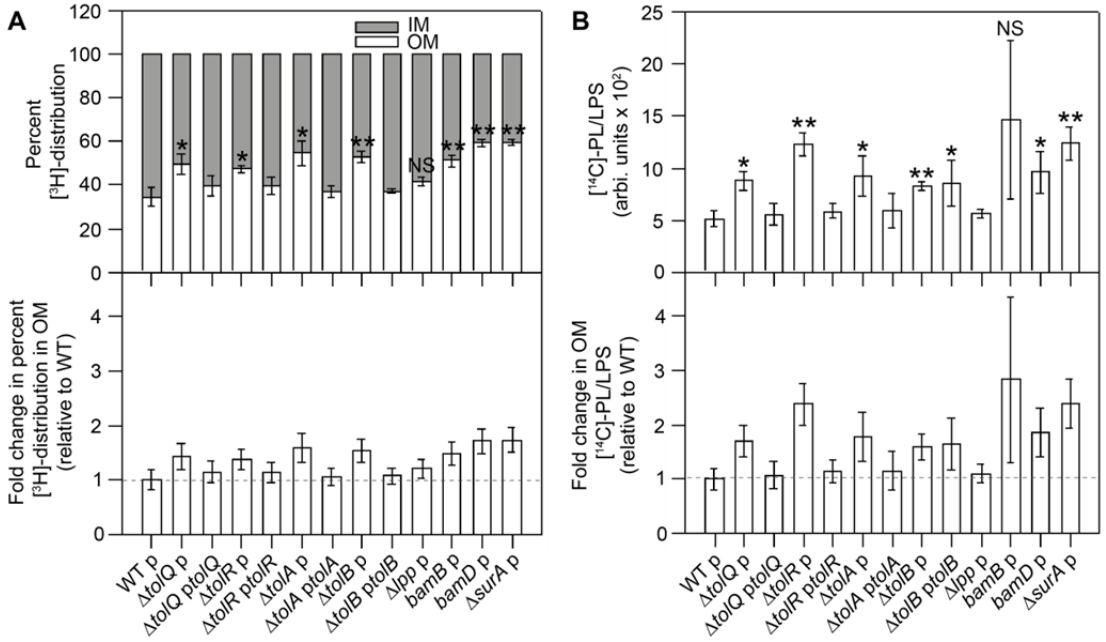

Figure 2 Cells lacking the Tol-Pal complex accumulate excess PLs (relative to LPS) in the OM. (**A**) Steady-state distribution of [^{3}H]-glycerol labelled PLs between the IM and the OM of WT, Δ*tol-pal*, and various mutant strains (*upper panel*)(Figure 2 - figure supplement 2). Distribution of [^{3}H]-labelled PLs in the OMs of respective mutants expressed as fold changes relative to the WT OM (*lower panel*). The IMs and OMs from both WT and *tol-pal* mutants were separated with equal efficiencies during sucrose density gradient fractionation (Figure 2 - figure supplement 1). (**B**) Steady-state PL:LPS ratios in the OMs of WT, Δ*tol-pal*, and various mutant strains (*upper panel*). Lipids were labelled with [^{14}C]-acetate and differentially extracted from OMs (Figure 2 - figure supplement 3). OM PL:LPS ratios of respective mutants expressed as fold changes relative to that in the WT OM (*lower panel*). Error bars represent standard deviations calculated from triplicate experiments. Student's t-tests: * $p < 0.05$; ** $p < 0.005$; NS, not significant (as compared to WT).

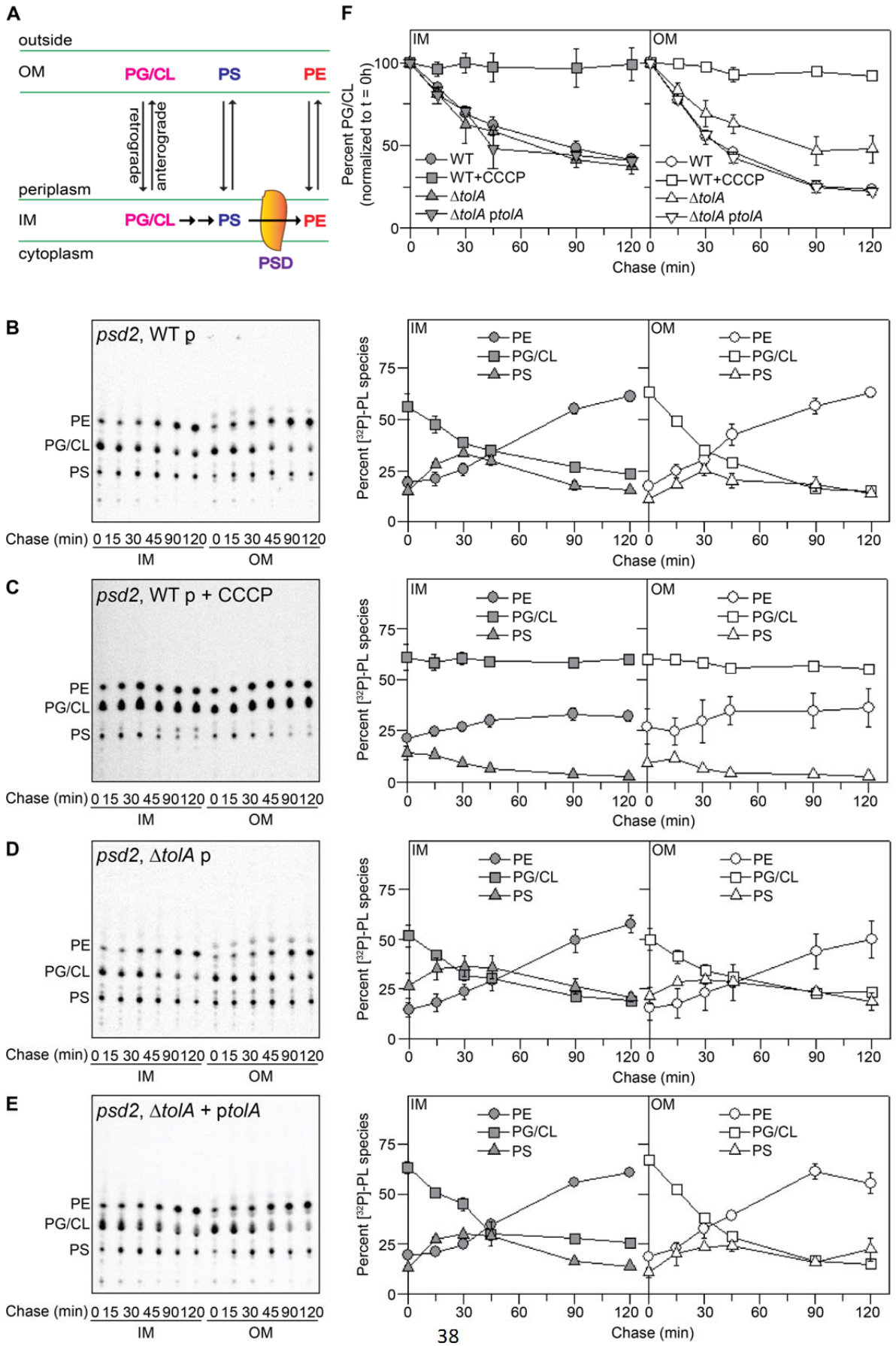
A
outside
OM
PG/CL
PS
PE
retrograde
anterograde
periplasm
IM
PG/CL
PS
PE
cytoplasm
PSD
F
IM
OM
Percent PG/CL (normalized to t = 0h)
WT
WT+CCCP
ΔtolA
ΔtolA ptolA
Chase (min)
B
psd2, WT p
PE
PG/CL
PS
Chase (min) 0 15 30 45 90 120 0 15 30 45 90 120
IM
OM
Percent [32P]-PL species
C
psd2, WT p + CCCP
D
psd2, ΔtolA p
E
psd2, ΔtolA + ptolA

752

Figure 3 Cells lacking the Tol-Pal complex are defective in OM PG/CL turnover. (**A**) A schematic diagram depicting movement and turnover of PE, PG and CL (major), and PS (trace) in the cell envelope. (**B-E**) TLC time-course analyses of [^{32}P]-pulse-labelled PLs extracted from the IMs and OMs of (**B**) WT, (**C**) WT (with CCCP added), (**D**) Δ*tolA*, and (**E**) *tolA*-complemented strains also harboring the *psd2* mutation. The average percentage levels of PE, PG/CL, and PS in the IM and OM at each time point, together with standard deviations, were quantified from triplicate experiments and shown on the right. (**F**) The percentage levels of PG/CL in the IMs and OMs from (**B-E**) normalized to the corresponding levels at the start of the chase (0 min).

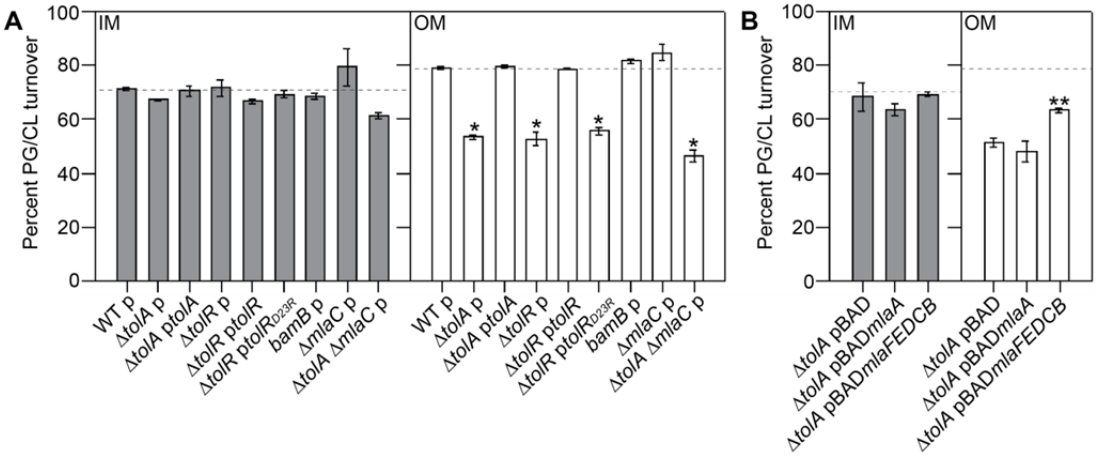

Figure 4 Tol-Pal function is required for efficient retrograde PG/CL transport, as judged by OM PG/CL turnover rates. Single time-point (2-h chase) quantification of the turnover rate of [^{32}P]-labelled PG/CL in the IMs and OMs of (**A**) WT, *tol-pal* and various mutant strains, and (**B**) Δ*tolA* overexpressing OmpC-Mla components, all in the *psd2* background (*see text*) (Figure 4-figure supplement 1). Percentage PG/CL turnover at 2-h is expressed as $[(\%PG/CL)_{start} - (\%PG/CL)_{2h}]/[(\%PG/CL)_{start}]$. Average percentage lipid levels and standard deviations were quantified from triplicate experiments. Student's t-tests: * $p < 0.0005$ as compared to WT; ** $p < 0.0005$ as compared to Δ*tolA*.

Figure supplements

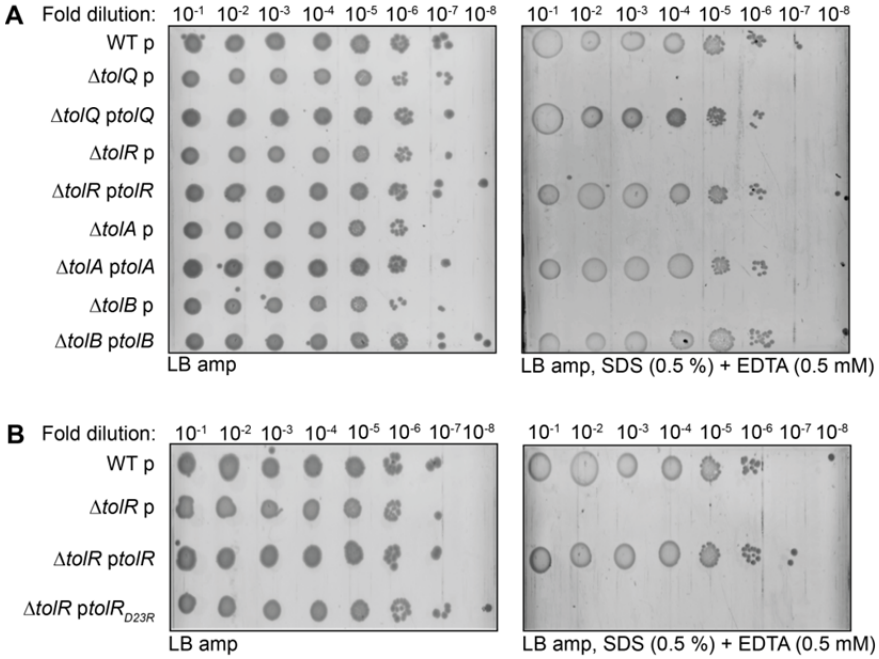

Figure 1 - figure supplement 1 SDS/EDTA sensitivity in *tol-pal* strains can be rescued only by expressing the corresponding functional *tol-pal* gene(s) from the pET23/42 plasmid (Wu et al., 2006). Serial dilutions of cultures of wild-type (WT) and indicated *tol-pal* strains harboring pET23/42 empty vector (p), or pET23/42 encoding (**A**) functional or (**B**) non-functional *tol-pal* gene(s) (e.g. p*tolA*), were spotted on LB agar plates containing 125 μg ml^{-1} ampicillin, supplemented with or without SDS (0.5%) and EDTA (0.5 mM) as indicated, and incubated overnight at 37˚C. In the plasmids used, the *tol-pal* gene(s) is placed under the control of the T7 promoter, which is transcribed at low levels by endogenous polymerases. $tolR_{D23R}$ is a non-functional allele encoding TolR protein that is defective in transducing energy derived from the pmf (Cascales et al., 2001).

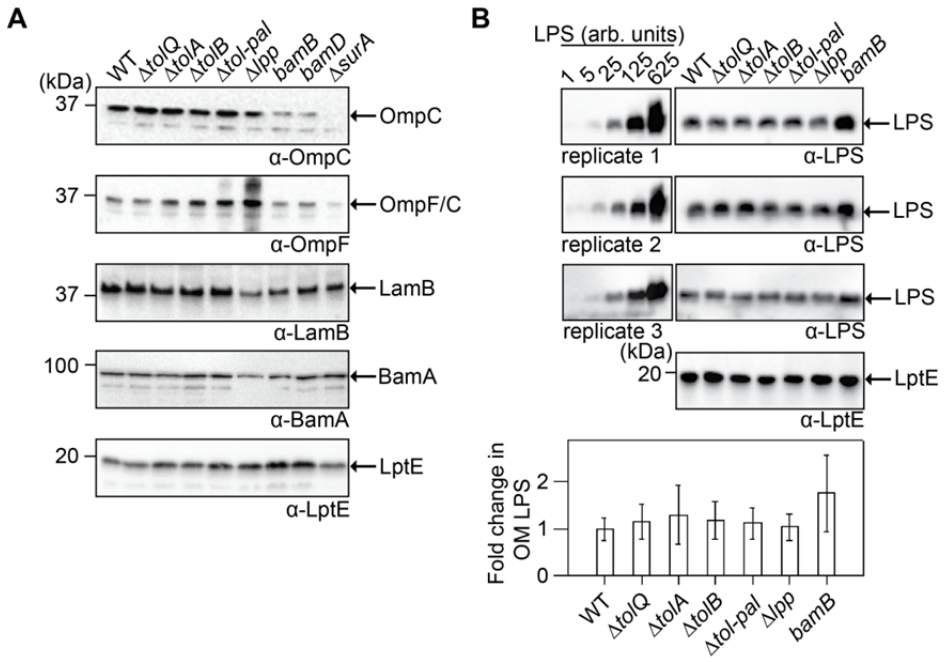

Figure 1 - figure supplement 2 *tol-pal* mutations do not affect β-barrel OMP and LPS assembly. Immunoblot analyses of (**A**) indicated OMPs and (**B**) LPS in the OMs of WT and *tol-pal* strains. Equal amounts of OMs (based on protein content) were resolved on SDS-PAGE prior to immunoblotting. The OMP assembly mutants (*bamB*, *bamD*, Δ*surA*) serve as controls for decreased OMP levels, and the levels of LptE serve as a loading control. α-LPS immunoblots were repeated three times for the same OM samples as shown. Serial dilutions of WT OMs were ran as standards and immunoblotted alongside the indicated samples, and LPS levels in these samples were quantified using ratio standard curves generated from the standards (Pitre et al., 2007). The relative levels of LPS in each OM was normalized to the WT OM, and averaged across all three technical replicates. Error bars represent standard deviations.

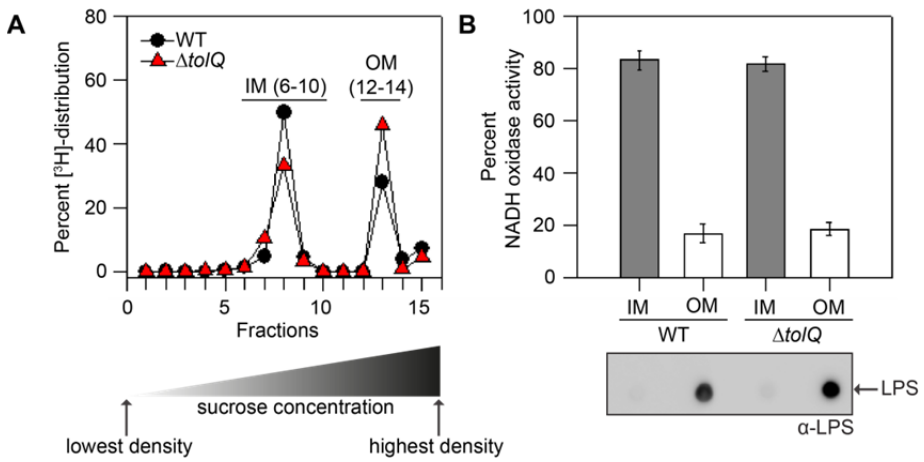

Figure 2 - figure supplement 1 Inner and outer membranes of both WT and *tol-pal* strains are effectively separated via fractionation on sucrose density gradients. (**A**) [^{3}H]-distribution profiles of WT (*black circles*) and Δ*tolQ* mutant (*red triangles*) cell lysates fractionated on a sucrose density gradient. Cells were grown in the presence of [2-^{3}H]-glycerol to specifically label PLs in the IM and OMs. (**B***)* Percent NADH oxidase activity (*upper panel*) and LPS levels (*lower panel*) (dot blot) in pooled IM and OM fractions from (**A**).

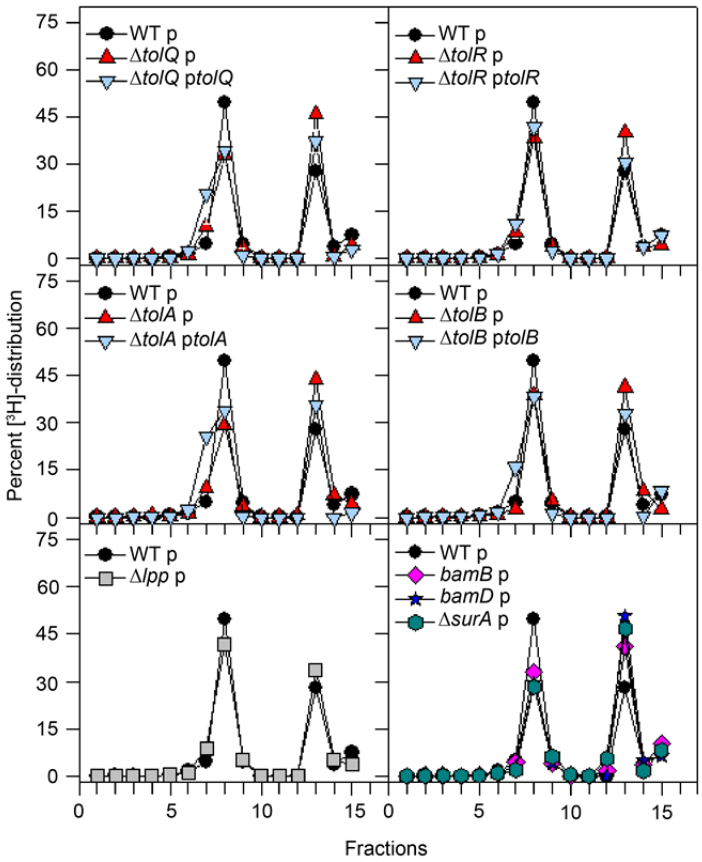

Figure 2 - figure supplement 2 Cells lacking the Tol-Pal complex contain more PLs in the OM, compared to the IM. Representative [^{3}H]-distribution profiles of cell lysates from WT (*black circles*), *tol-pal* mutants (*red triangles*), *tol-pal*-complemented strains (*blue inverted triangles*), and various control strains, fractionated on sucrose density gradients. Cells were grown in the presence of [2-^{3}H]-glycerol to specifically label PLs in the IMs and OMs. Total [^{3}H]-activities detected in IM (6-10) and OM (12-14) fractions were expressed as a percentage of their sums, averaged across three replicate experiments, and plotted in Figure 2A.

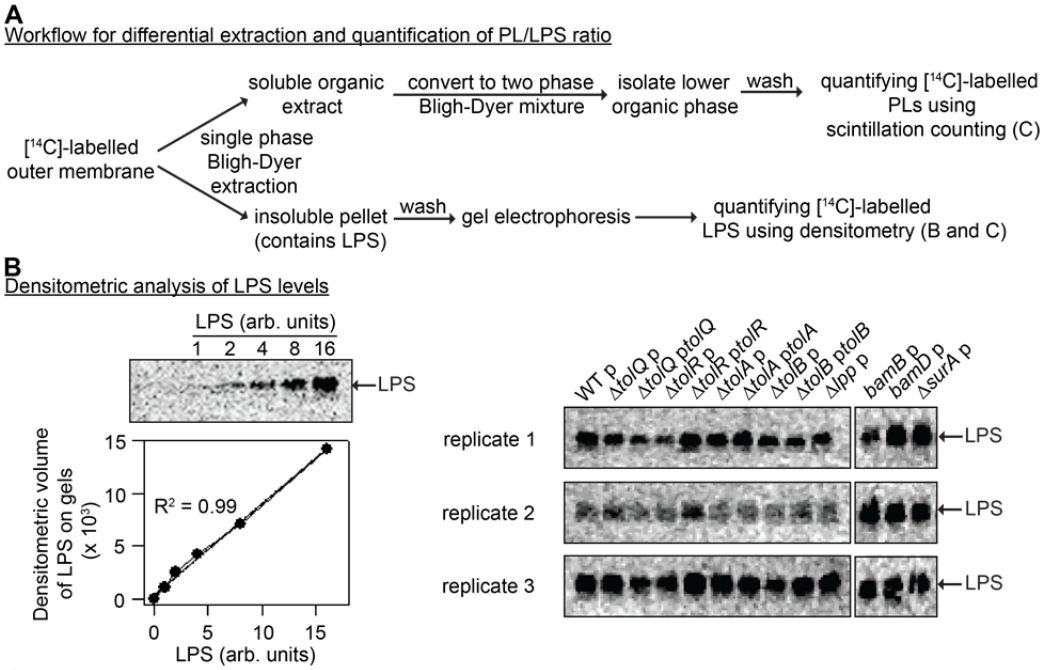

C
Tabulation of [14C]-labelled PLs and LPS levels

Strains	Replicate 1			Replicate 2			Replicate 3			Average	
	PL	LPS	PL/LPS	PL	LPS	PL/LPS	PL	LPS	PL/LPS	PL/LPS	SD
WT p	3640	7.3	497	1517	2.5	597	3602	7.9	457	517	72
Δ*tolQ* p	3715	4.3	860	3014	3.1	975	6471	8.1	797	877	91
Δ*tolQ ptolQ*	1970	3.0	663	1321	2.4	548	1990	4.4	457	556	103
Δ*tolR* p	3448	2.6	1306	3452	2.7	1279	6215	5.6	1110	1231	106
Δ*tolR ptolR*	6076	9.2	661	2147	4.1	526	6062	10.5	577	588	68
Δ*tolA* p	5342	5.6	961	2971	2.7	1092	5218	7.4	709	921	195
Δ*tolA ptolA*	3508	8.6	406	1987	2.9	688	4250	6.2	691	595	163
Δ*tolB* p	3672	4.4	838	2214	2.6	868	3300	4.2	782	830	44
Δ*tolB ptolB*	4184	4.2	1006	3014	3.2	957	3890	6.4	610	857	216
Δ*lpp* p	2871	5.0	578	1784	3.0	599	3362	6.4	524	567	38
bamB p	6622	2.8	2340	6806	6.2	1105	6624	7.0	944	1463	764
bamD p	5784	7.7	753	6188	6.3	985	6252	5.5	1143	960	196
Δ*surA* p	7004	5.0	1401	7314	6.8	1076	7528	6.1	1236	1238	163

Figure 2 - figure supplement 3 Cells lacking the Tol-Pal complex accumulate excess PLs (relative to LPS) in the OM. (**A***)* Workflow for differential extraction and subsequent quantification of PLs and LPS levels in the [^{14}C]-acetate labelled OMs. (**B***)* In-gel quantification of [^{14}C]-LPS levels in the OMs of WT, *tol-pal* mutants, *tol-pal*-complemented strains, and various control strains. [^{14}C]-LPS of respective strains separated on SDS-PAGE gels (*right*) were visualized by phosphor imaging and quantified via densitometry using a linear standard curve (*left*). (**C**) Tabulation of [^{14}C]-labelled PL levels (scintillation counts), LPS levels (gel

819 densitometry), and arbitrary PL/LPS ratios in the OMs of the indicated strains. The average
820 PL/LPS ratio for each strain was obtained from three independent experiments, and plotted in
821 Figure 2B.

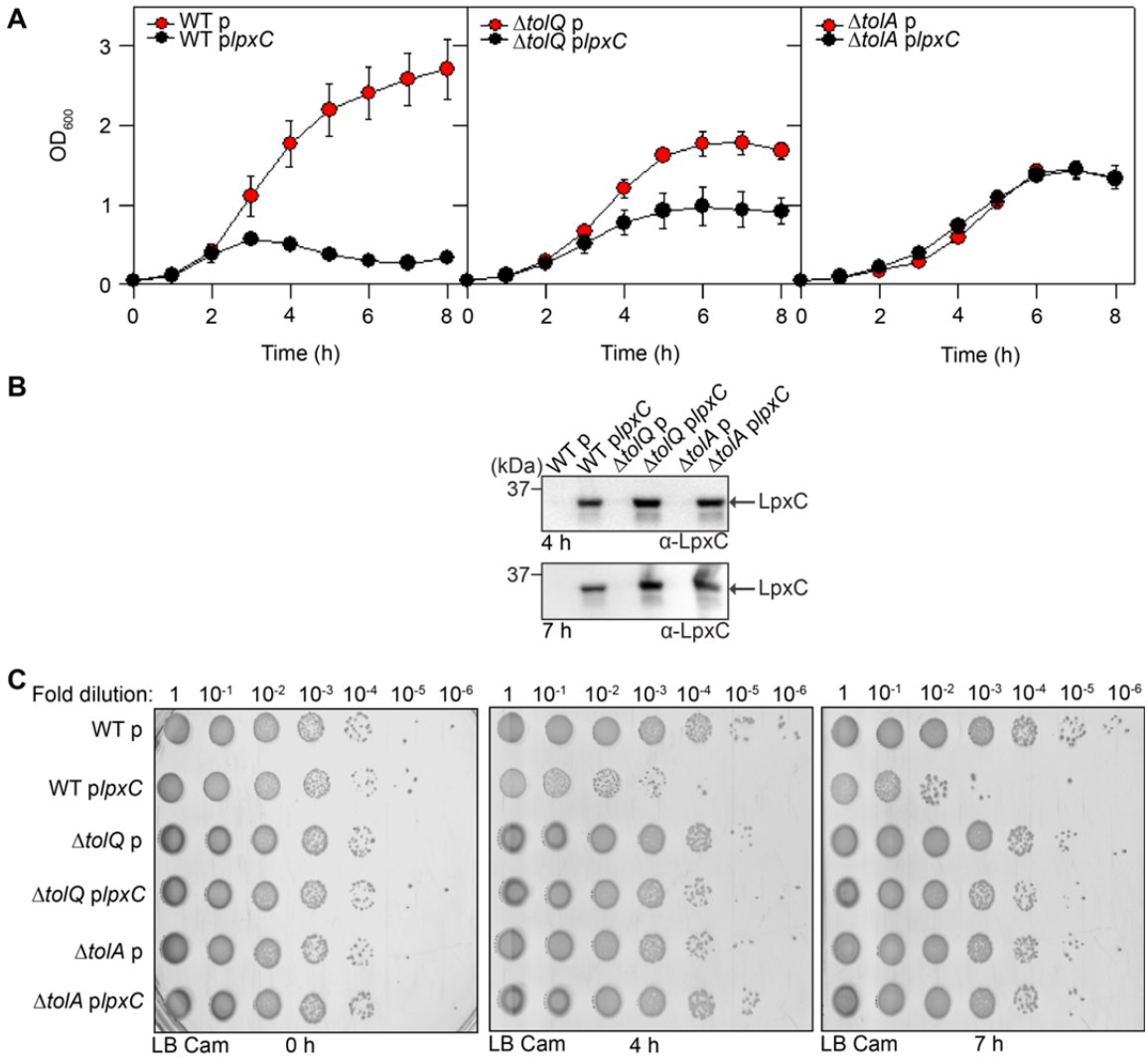

Figure 2 - figure supplement 4 *tol-pal* mutants survive toxicity induced by overproduction of LpxC, the enzyme catalyzing the first committed step in LPS biosynthesis. (**A**) Growth profiles of WT, Δ*tolQ* and Δ*tolA* cells harboring either pBAD18cm empty vector (p) or pBAD18cm*lpxC* (p*lpxC*) and grown in the presence of arabinose (0.2%). OD_{600} values were measured every hour during growth. Error bars represent the standard deviation observed from triplicate experiments. (**B**) Immunoblot analyses of LpxC in the respective strains from 4-h and 7-h cultures in (**A**), indicating comparable levels of LpxC overexpression in these strains. (**C**) Indicated serial

830 dilutions of 0-, 4- and 7-h cultures of the same strains in (**A**) were spotted on LB agar plates

831 containing 30 μg ml^{-1} cam and incubated overnight at 37˚C.

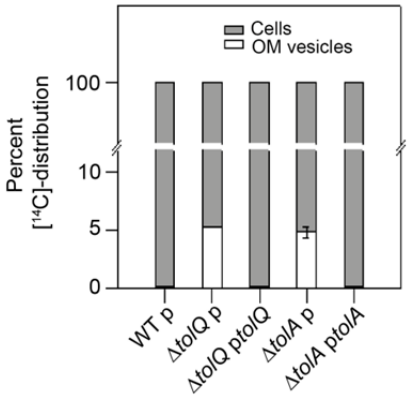

Figure 2 - figure supplement 5 Cells lacking the Tol-Pal complex release OM vesicles amounting to ~5% of total cellular membrane material. Average steady-state distribution of [^{14}C]-lipids found associated with cells (total membranes) or OM vesicles for WT, *tol-pal* mutants and complemented strains. Error bars represent the standard deviation calculated from triplicate experiments.

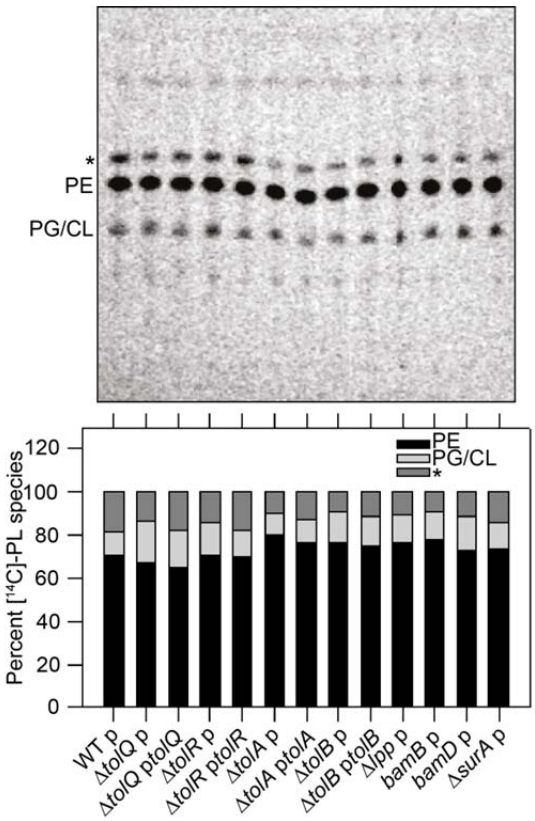

Figure 2 - figure supplement 6 Although cells lacking the Tol-Pal complex accumulate ~50% more PLs in the OM, PL compositions of this membrane are comparable to that in WT cells. TLC analysis of [^{14}C]-labelled PLs extracted from the OMs of WT and indicated mutant strains. Equal amounts of radioactivity were spotted for each sample. An unidentified lipid species that migrated in this solvent system similarly to palmitoylated PG (Dalebroux et al., 2014) is annotated by an asterisk (*). The percentage levels of PE, PG/CL, and the unidentified lipid were quantified and shown below.

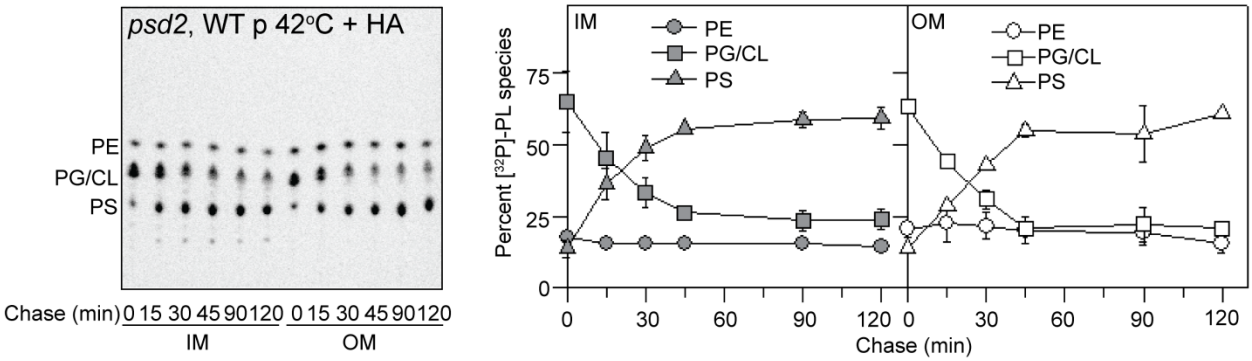

Figure 3 - figure supplement 1 PG/CL is converted to PS in the absence of PSD function. TLC time-course analyses of [^{32}P]-pulse-labelled PLs extracted from the IMs and OMs of the WT strain also harboring the temperature-sensitive *psd2* mutation. Cells were incubated at the restrictive temperature (42˚C, 4 h) and PLs were pulse-labelled with [^{32}P]-phosphate during the last 30 min at the restrictive temperature, and then chased in the presence of excess cold phosphate and hydroxylamine (HA; 10 mM) at the same temperature. HA is a known PSD inhibitor (Satre and Kennedy, 1978). The percentage levels of PE (circles), PG/CL (squares), and PS (triangles) in the IM (grey symbols) and OM (white symbols) at each time point were quantified and shown on the right. The results clearly showed quantitative PG/CL to PS conversion.

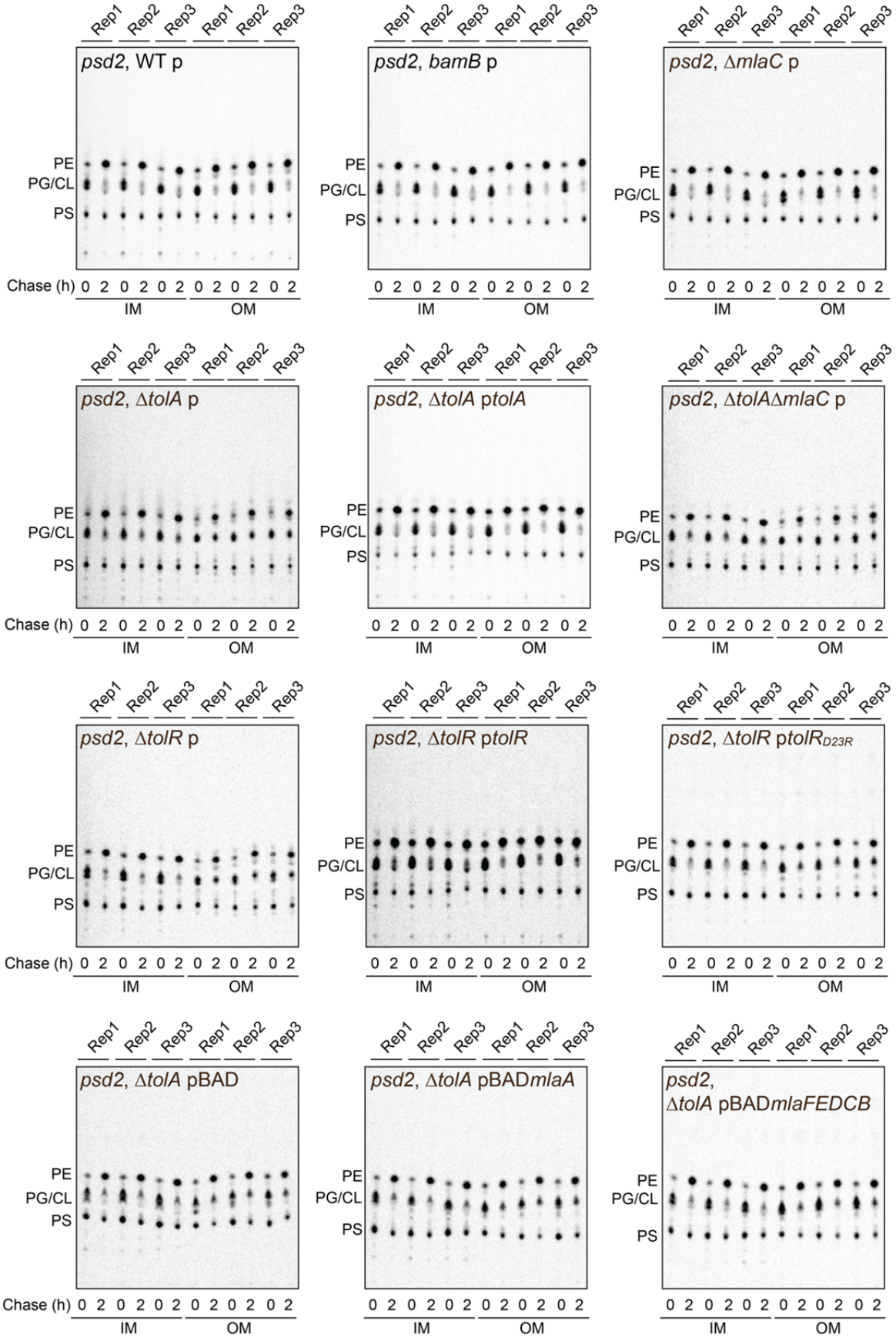
Rep1 Rep2 Rep3 Rep1 Rep2 Rep3
psd2, WT p
psd2, bamB p
psd2, ΔmlaC p
psd2, ΔtolA p
psd2, ΔtolA ptolA
psd2, ΔtolAΔmlaC p
psd2, ΔtolR p
psd2, ΔtolR ptolR
psd2, ΔtolR ptolR$_{D23R}$
psd2, ΔtolA pBAD
psd2, ΔtolA pBADmlaA
psd2, ΔtolA pBADmlaFEDCB
PE
PG/CL
PS
Chase (h) 0 2 0 2 0 2 0 2 0 2 0 2
IM
OM

857

Figure 4 - figure supplement 1 Cells lacking the Tol-Pal complex are defective in OM PG/CL turnover. Single time-point TLC analyses of [^{32}P]-pulse-labelled PLs extracted from the IMs and OMs of indicated strains also harboring the temperature-sensitive *psd2* mutation. Cells were incubated at the restrictive temperature (42˚C, 4 h) and PLs were pulse-labelled with [^{32}P]-phosphate during the last 30 min at the restrictive temperature, and then chased in the presence of excess cold phosphate at the permissive temperature (30˚C) for 2 h. The average extents of PG/CL turnover ([$(\%PG/CL)_{start}$ – $(\%PG/CL)_{2h}$]/[$(\%PG/CL)_{start}$]) in the IM and OM for each strain was obtained from three biological replicate (Reps) experiments, and plotted in Figure 4.

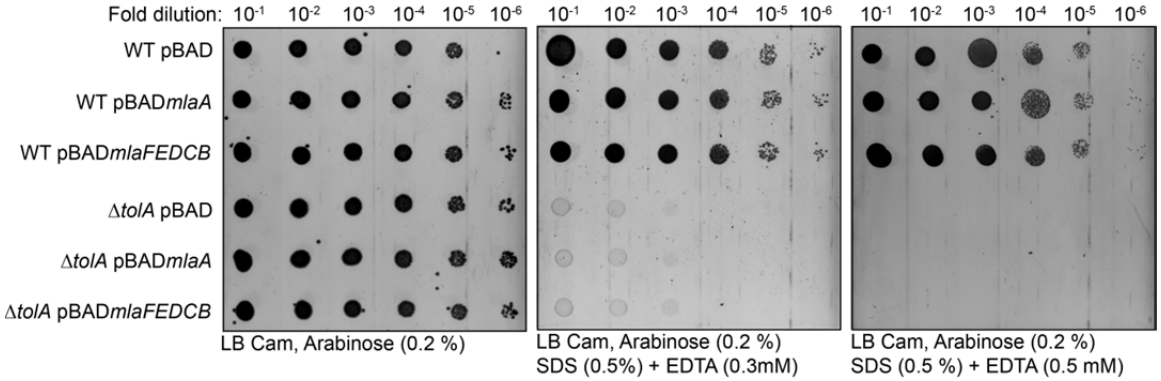

Figure 4 - figure supplement 2 Overexpression of OmpC-Mla components does not rescue SDS/EDTA sensitivity of the Δ*tolA* mutant. Serial dilutions of cultures of wild-type (WT) and the Δ*tolA* mutant strain (both in the *psd2* background) harboring pBAD33 empty vector (pBAD) or pBAD33 encoding indicated components of the OmpC-Mla system, were spotted on LB agar plates containing chloramphenicol (30 μg ml^{-1}) and arabinose (0.2 %), supplemented with or without SDS (0.5%) and EDTA (0.3/0.5 mM) as labeled, and incubated overnight at the permissive temperature (30˚C).

Supplementary File 1

Supplementary File 1A. Bacterial strains used in this study.

Strains	Relevant genotype	References
MC4100	[*F⁻ araD139* Δ*(argF-lac) U169 rpsL150 relA1 flbB5301 ptsF25 deoC1 ptsF25 thi*]	Casadaban, 1976
BW25113	*F-* Δ*(araD-araB)567* Δ*lacZ4787::rrnB-3 λ- rph-1* Δ*(rhaDrhaB)568 hsdR514*	Datsenko and Wanner, 2000
NovaBlue	*endA1 hsdR17 (rK12– mK12+) supE44 thi-1 recA1 gyrA96 relA1 lac F' [proA+B+lacIqZ*Δ*M15::Tn10]*	Novagen
NR754	MC4100 *araD*$^{+}$	Ruiz et al., 2008
EH150	*psd-2 purA*$^{+}$; temperature-sensitive PSD	Hawrot and Kennedy, 1978
NR1215	NR754 Δ*surA*	Ruiz et al., 2010
NR698	MC4100 *lptD4213* (*carB*$^{+}$, *Tn10*)	Ruiz et al., 2005
NR814	MC4100 *bamD::kan*	Wu et al., 2005
NR721	MC4100 *bamB::kan*	Ruiz et al., 2005
RS101	BW25113 Δ*tolQ::kan*	This study
JW0728	BW25113 Δ*tolR::kan*	Baba et al., 2006
RS102	BW25113 Δ*tolA::kan*	This study
JW5100	BW25113 Δ*tolB::kan*	Baba et al., 2006
RS104	BW25113 Δ*tol-pal::kan*	This study
RS105	BW25113 Δ*lpp::kan*	This study
RS119	MC4100 Δ*tolQ::kan*	This study
RS120	MC4100 Δ*tolR::kan*	This study
RS121	MC4100 Δ*tolA::kan*	This study
RS122	MC4100 Δ*tolB::kan*	This study
RS125	MC4100 Δ*tol-pal::kan*	This study
RS137	MC4100 Δ*lpp::kan*	This study
CZS011	MC4100 Δ*mlaC::kan*	Lab collection
RS173	EH150 Δ*tolR::kan*	This study
RS174	EH150 Δ*tolA::kan*	This study
RS177	EH150 *bamB::kan*	This study
RS178	EH150 Δ*mlaC::kan*	This study
RS180	EH150 Δ*tolA* Δ*mlaC::kan*	This study
JXE082	NR754 Δ*tolQ::kan*	This study
JXE081	NR754 Δ*tolA::kan*	This study

878 **Supplementary File 1B. Plasmids used in this study.**

Plasmids	Description	Plasmid construction		References
		PCR template[a]	PCR primers[b]	
pET23/42	P_{T7} inducible expression vector, contains multiple cloning site of pET42a(+) in pET23a(+) backbone; Amp^R	-	-	Wu et al., 2006
pBAD18cm	P_{BAD} inducible expression vector; Cam^R	-	-	Guzman et al., 1995
pBAD33	P_{BAD} inducible expression vector; Cam^R	-	-	Guzman et al., 1995
pET23/42*tolQ*	Encodes full length TolQ; Amp^R	Ch. DNA	TolQ-N-NdeI/TolQ-C-AvrII	This study
pET23/42*tolR*	Encodes full length TolR; Amp^R	Ch. DNA	TolR-N-NdeI/TolR-C-AvrII	This study
pET23/42$tolR_{D23R}$	Encodes full length $TolR_{D23R}$; Amp^R	pET23/42*tolR*	TolR-D23R-N/TolR-D23R-C	This study
pET23/42*tolA*	Encodes full length TolA; Amp^R	Ch. DNA	TolA-N-NdeI/TolA-C-AvrII	This study
pET23/42*tolB*	Encodes full length TolB; Amp^R	Ch. DNA	TolB-N-NdeI/TolB-C-AvrII	This study
pET23/42*tol-pal*	Encodes full Tol-Pal complex; Amp^R	Ch. DNA	TolQ-N-NdeI/Pal-C-AvrII	This study
pBAD18cm*lpxC*	Encodes full length LpxC; Cam^R	Ch. DNA	LpxC-N-KpnI/LpxC-C-XbaI	This study
pBAD33*mlaA*	Encodes full length MlaA; Cam^R	Ch. DNA	MlaA-N-KpnI/MlaA-C-XbaI	This study
pBAD33*mlaFEDCB*	Encodes full length MlaFEDCB; Cam^R	Ch. DNA	MlaFEDCB-N-KpnI/MlaFEDCB-C-XbaI	This study

879 [a] Ch. DNA = MC4100 chromosomal DNA.
880 [b] Primer sequences are listed in Supplementary File 1C.

881 **Supplementary File 1C. List of oligonucleotides**

Primer name	Sequence (5'-3')[a]
TolQ-N-NdeI	AGCACATATGACTGACATGAATATCC
TolQ-C-AvrII	ATTCCTAGGTTACCCCTTGTTGCTCTC
TolR-N-NdeI	ACATCATATGGCCAGAGCGCGTGGAC
TolR-C-AvrII	ACACCTAGGTTAGATAGGCTGCGTC
TolA-N-NdeI	ACATCATATGTCAAAGGCAACCGAACAAAAC
TolA-C-AvrII	ACTACCTAGGTTACGGTTTGAAGTCC
TolB-N-NdeI	GCGAATTCATATGAAGCAGGCATTACGAGTA
TolB-C-AvrII	ACTACCTAGGTCACAGATACGGCG
Pal-C-AvrII	ACTACCTAGGTTAGTAAACCAGTACC
LpxC-N-KpnI	ATAAGGTACCTAATTTGGCGAGATAATACGATGATCAAA
LpxC-C-XbaI	ATCGTCTAGATTATGCCAGTACAGCTGAAGG
MlaA-N-KpnI	ATAAGGTACCAAAAAAACAGGGAGACATTTATGAAGCTTC
MlaA-C-XbaI	ATCGTCTAGATTATTCAGAATCAATATCTTTTAAAT
MlaFEDCB-N-KpnI	ATAAGGTACCCGCAAGACGAAGGGTGAATTATGGAGCAGT
MlaFEDCB-C-XbaI	ATCGTCTAGATTAACGAGGCAGAACATCAGCAGG
TolR-D23R-N	ATTGTACCGTTGCTGAGAGTACTGCTGGTGCTG
TolR-D23R-C	CAGCACCAGCAGTACTCTCAGCAACGGTACAAT

882 [a] restriction sites are underlined.